Trop J Nat Prod Res, February 2026; 10(2): 7429 - 7444 ISSN 2616-0684 (Print)
ISSN 2616-0692 (Electronic)

Tropical Journal of Natural Product Research

Available online at https://www.tjnpr.org

Original Research Article

Effects of *Celosia argentea* L. leaf on Monosodium Glutamate (MSG)-Induced Uterine Leiomyoma In Wistar Rats: Experimental and Computational Perspectives

Akingbolabo D. Ogunlakin[1]*, Oluwafemi A. Ojo[1,13], Peluola O. Ayeni[1], Gideon A. Gyebi[2], Amel Elbasyouni[3], Oyindamola E. Awosola[4], Moyosoluwa M. Dada[5], Mamta Bisht[6], Edema A. Adeleye[7], Oluwadamilola G. Adedoyin[1], Opeyemi J. Akinmurele[8], Abdullahi A. Adegoke[9], Ajibola D. Adelakun[10], Omolola Oluwadara[11], Jumoke Ilo[12], Ochuko L. Erukainure [14], Seun E. Kuyoro[15], Oluyomi S. Adeyemi[1]

[1]*Phytomedicine and Drug Discovery Research Laboratory (PDD-RL), Biochemistry Programme, Bowen University, Iwo, 232101, Nigeria*
[2]*Department of Biotechnology and Food Science, Faculty of Applied Sciences, Durban University of Technology, P.O. Box 1334, Durban 4000, South Africa.*
[3]*Department of Molecular Biology and Biotechnology, Pan African University for Basic Sciences, Technology and Innovation (PAUSTI), Nairobi, Kenya*
[4]*Next Era Health, Julius Kadir Street, Ifako-Gbagada, Lagos, Nigeria*
[5]*Anatomy Department, Babcock University, Ilishan Remo, Ogun State, Nigeria*
[6]*Department of Chemistry, School of Applied and Life Science, Uttaranchal University, Dehradun, India.*
[7]*Chemistry and Biochemistry Department, The University of Tulsa, Oklahoma, USA*
[8]*Department of Pharmacognosy, Lead City University, Ibadan. Ibadan. Nigeria*
[9]*Department of Pharmacognosy, University of Ibadan, Ibadan. Nigeria*
[10]*Department of Pharmaceutical Sciences, University of Arizona, Arizona, USA*
[11]*Project Development and Design Department, Federal Institute of Industrial Research, Oshodi, Lagos State, Nigeria.*
[12]*Human Nutrition and Dietetics Department, College of Health Science, Osun State University, Osogbo, Osun State. Nigeria*
[13]*Research Centre for Integrative Physiology and Pharmacology and Turku Center for Disease Modeling, Institute of Biomedicine, University of Turku, Turku, Finland*
[14]*Laser Research Centre, Faculty of Health Sciences, University of Johannesburg, Doornfontein 2028, South Africa.*
[15]*Biological Sciences Department, University of Massachusetts, Lowell. USA*

ARTICLE INFO

Article history:
Received 04 January 2026
Revised 17 January 2026
Accepted 19 January 2026
Published online 01 March 2026

ABSTRACT

Uterine leiomyomas, commonly known as fibroids, affect nearly 30% of women of reproductive age and are linked to infertility, type II diabetes, and psychological stress. Recent studies highlight somatic mutations and cytogenetic abnormalities, including transcriptional dysregulation of DUSP6, as potential biomarkers for early detection and intervention. *Celosia argentea*, a leafy edible plant long valued in traditional medicine, was investigated in this study for its antioxidant, antidiabetic, and protective effects against monosodium glutamate (MSG)-induced uterine leiomyoma in Wistar rats, with mechanisms explored through *in silico* analysis. Female rats were administered MSG for 30 days to induce fibroids, followed by daily treatment with 100 mg/kg of *C. argentea* aqueous leaf extract for 30 days. Biochemical assays measured lipid peroxidation, acetylcholinesterase (AChE), monoamine oxidase (MAO), and reproductive hormones, while histopathology examined uterine tissues. *In vitro* tests assessed antioxidant activity and enzyme inhibition (MAO and AChE), and High-Performance Liquid Chromatography (HPLC) identified chlorogenic acid and rutin, which were docked against DUSP6 computationally. Antioxidant assays revealed modest radical scavenging and iron-chelating activity, alongside concentration-dependent inhibition of α-amylase, α-glucosidase, and acetylcholinesterase. The extract also inhibited monoamine oxidase (MAO) with an IC_{50} of 0.098 ± 0.005 µg/mL, comparable to donepezil. Hormonal assays showed significant correction of elevated testosterone and estradiol levels. Molecular docking confirmed strong binding affinities of rutin and chlorogenic acid to DUSP6, which supported the antifibrotic potential of *C. argentea.* Overall, *C. argentea* demonstrated the ability to modulate multiple pathways, suggesting therapeutic promise in restoring hormonal balance and uterine health in fibrotic conditions.

Keywords: Uterine leiomyoma; Phytotherapy; *Celosia argentea;* Hormonal imbalance, DUSP6.

Introduction

Uterine leiomyomas (fibroids), which are tumors derived from uterine smooth muscle cells, are the most common type of gynecologic neoplasm.[1]

*Corresponding author. E mail: gbolaogunlakin@gmail.com
Tel: +2347037883049

Citation: Ogunlakin AD, Ojo OA, Ayeni PO, Gyebi GA, Elbasyouni A, Awosola OE, Dada MM, Bisht M, Adeleye EA, Adedoyin OG, Akinmurele OJ, Adegoke AA, Adelakun AD, Oluwadara O, Ilo J, Erukainure OL, Kuyoro SE, Adeyemi OS. Effects of *Celosia Argentea* L. Leaf on Monosodium Glutamate (MSG)-Induced Uterine Leiomyoma In Wistar Rats: Experimental and Computational Perspectives. Trop J Nat Prod Res. 2026; 10(2): 7429 – 7444 https://doi.org/10.26538/tjnpr/v10i2.53

Official Journal of Natural Product Research Group, Faculty of Pharmacy, University of Benin, Benin City, Nigeria

About 70 % of women of reproductive age have uterine leiomyomas.[2] Although uterine leiomyomas are benign tumors, they can lead to complications such as menorrhagia, dysmenorrhea, anemia, infertility, and miscarriage.[1] According to Aninye *et al*.,[3] risk factors for uterine leiomyomas include age, family history, ethnicity, obesity, poor nutrition, physical inactivity, exposure to certain chemicals (e.g., monosodium glutamate), and the use of some prescription drugs that may elevate total protein, cholesterol, and estradiol levels. Additionally, a strong association has been observed
between uterine leiomyomas and an increased risk of type II diabetes in young women.[4] Regional variations exist in Southwest Nigeria; approximately 79.9 % of women had multiple leiomyomas, compared to 48.8 % in Northern Nigeria.[5]

Diagnosis remains challenging due to variable clinical features. To better understand the molecular pathogenesis of leiomyomas, researchers have been investigating specific biomarkers. Uterine leiomyoma is a monoclonal tumor that starts in a single cell.[6-8] Thus,

cytogenetic anomalies and somatic mutations are anticipated to become useful biomarkers.[7] These included ten (10) hypermethylated genes and two (2) hypomethylated genes. These are leiomyoma-specific marker genes.[9] Oxidative stress and inflammation-induced DNA damage result in genetic changes that promote carcinogenesis.[10] Unchecked cell survival and proliferation are encouraged by the cytokine- and growth factor-rich environment created by chronic inflammation.[11] Hormonal abnormalities that disrupt normal cellular signaling pathways exacerbate this process.[12] The side effects and temporary symptomatic relief of orthodox pharmaceuticals necessitate a better treatment alternative that is less risky and detrimental to the individual, as well as one that is readily accessible and relatively less expensive.[13,14]

Nutraceuticals, which include fruits and vegetables, are food-based natural medicine.[15,16] *Celosia argentea*, sometimes called silver cock's comb (Family: Amaranthaceae), is a flowering plant that grows extensively throughout tropical and subtropical areas.[17] Because of its litholytic, nephroprotective, anti-inflammatory, and diuretic qualities, it is widely used in traditional medicine in Asia, Africa, and South America.[17] This plant's therapeutic usefulness is attributed to its abundance of bioactive substances. *C. argentea* has long been used in African herbal medicine, Indian Ayurveda, and Traditional Chinese Medicine (TCM) to treat a variety of illnesses, including kidney problems, urinary tract infections, and urolithiasis (kidney stones).[18,19] The medicinal plant *Celosia argentea* is full of bioactive substances that provide it with pharmacological qualities such as nephroprotective, antioxidant, diuretic, and antilithiatic actions.[17] Flavonoids, saponins, alkaloids, tannins, and phenolic compounds are the main bioactive components of *C. argentea*, and each one adds to the plant's therapeutic advantages.[20] Therefore, this study evaluated the antioxidant, antidiabetic, and ameliorative potentials of the aqueous extract of *Celosia argentea* leaf on monosodium glutamate (MSG)-induced uterine leiomyoma in Wistar rats and provides evidence of their mechanisms of action using *in silico* approach.

Materials and Methods

Plant Collection and Extraction

Leaves of *Celosia argentea* harvested from Adediran Farm in the Gbandu area of Oluponna, Osun State, Nigeria, were thoroughly rinsed twice with distilled water to eliminate surface impurities and extraneous matter prior to further processing. Plant identification and authentication were performed at the Bowen University Herbarium, Iwo. A voucher specimen was prepared and deposited with the voucher number BUH056. Freshly pulverized leaves (500 g) were extracted with distilled water (4 L) at room temperature for 72 hr with intermittent stirring. The resulting mixture was filtered, and the filtrate was freeze-dried. The obtained dark green extract was stored at −4 °C until further use.

In vitro Antioxidant Assays

2,2-Diphenyl-1-picrylhydrazyl (DPPH) Scavenging Ability

The DPPH radical scavenging assay, using 2,2-diphenyl-1-picrylhydrazyl (DPPH), was performed according to the method described by Fadogba *et al.* [21] with minor modifications. In short, quantities of 10, 20, 30, and 40 mg/mL were used to make the extract. One milliliter of each concentration was combined with one milliliter of DPPH solution; two milliliters of DPPH solution devoid of extract served as the control. A UV-Vis spectrophotometer was used to detect absorbance at 516 nm after the reaction mixtures were incubated for 30 minutes at room temperature in the dark. Every measurement was done three times. The following formula was used to determine the percentage of DPPH radical scavenging activity:

$$\%\ \text{scavenging ability} = \frac{\text{Absorbance of reference} - \text{Absorbance of sample}}{\text{Absorbance of reference}} \text{x} \frac{100}{1}$$

Ferric Reducing Antioxidant Power (FRAP)

The extract's Ferric reducing power was determined using a modified procedure described by Ogunlakin *et al.* [23] was employed. The control (0 mg/mL) and 20, 30, and 40 mg/mL test tubes were each labelled as such. After transferring 200 µL to each test tube, 2 mL of 1% KFeCN and 2 mL of pH 6.6 phosphate buffer were added. The test tubes were then put in a water bath and incubated at 50 °C for 10 minutes. Following the incubation period, two milliliters of 10% TCA were added to each test tube. Two milliliters of the supernatant were moved to another test tube after the combination had been incubated for fifteen minutes. A spectrophotometer was used to measure the absorbance of the solution at 700 nm after 500 µL of 0.1% ferric chloride was added to each supernatant.

Fenton's reaction (OH Radical scavenging activity)

The Ogunlakin *et al.*[23] method was used to test the phenolics' capacity to stop Fe^{2+}/H_2O_2-induced deoxyribose breakdown. Briefly, test samples were combined with a reaction mixture that contained 120 µL of 20 mM deoxyribose, 400 µL of 0.1 M phosphate buffer, 40 µL of 20 mM hydrogen peroxide, and 40 µL of 500 µM $FeSO_4$. After that, distilled water was used to get the volume down to 800 µL. The reaction was stopped by adding 0.5 mL of 2.8% trichloroacetic acid (TCA) to the reaction mixture after 30 minutes of incubation at 37 °C. Next, 0.4 mL of a 0.6% thiobarbituric acid (TBA) solution was added. The tubes were then incubated in boiling water for 20 minutes. The absorbance at 532 nm was measured using a spectrophotometer. The following formula was then used to calculate the capacity to scavenge OH radicals as a percentage (%):

$$\%\ \text{scavenging ability} = \frac{\text{Absorbance of reference} - \text{Absorbance of sample}}{\text{Absorbance of reference}} \text{x} \frac{100}{1}$$

Determination of Fe^{2+} Chelating Ability

A reaction mixture comprising 168 µL of 0.1 M Tris–HCl (pH 7.4), 218 µL of saline, and the extracts (0–25 µL) was mixed with freshly generated 500 µM $FeSO_4$ (150 µL). After five minutes of incubation, 13 µL of 0.25% 1,10-phenanthroline (w/v) was added to the reaction mixture. A spectrophotometer was then used to measure the absorbance at 510 nm. The Fe2+ chelating ability was subsequently calculated.[22]

Nitric Oxide Scavenging Activity

The concept underlying the assay is that NO and/or its oxidative derivatives react with a non-fluorescent chemical to produce a fluorescent result.[22] 250 µL of 10 mM sodium nitroprusside was mixed with various amounts of the extract and ascorbic acid. Following 180 minutes of incubation at 25 °C, 500 µL of Griess reagent was added to the mixture, and the absorbance at 546 nm was measured. In the control samples, there is no extract or standard but 250 µL of sodium nitroprusside, phosphate-buffered saline, and Griess reagent.

Acetylcholinesterase (ACHE) Inhibitory Assay

The colorimetric approach was used to measure acetylcholinesterase activity.[23] 2,000 mL of 100 mM phosphate butter pH 8.0, 100 mL of test sample stock solution in methanol (final concentration of 42.5 µg/mL), 100 mL of enzyme AchE solution at final concentrations of 0.03 U/mL and 0.01 µg/mL, respectively, and 100 µL of DTNB (0.3 mM) prepared in 100 mM phosphate buffer at pH 7.0 containing 120 mM sodium bicarbonate made up the reaction assay mixture. After vortexing the reaction mixture, it was pre-incubated for 30 minutes at 37 °C in a water bath. As a negative control, 100 µL of ATCI or BTCI at a final concentration of 0.5 mM was then added to start the reaction. Methanol was used in place of the inhibitor solution. After that, the absorbance change at λmax 412 nm was recorded for five minutes at room temperature. Every assay was performed in triplicate. The sample's ultimate concentration was 42.5 µg/mL. At the same concentration, donepezil served as a positive control. The percentage of inhibition was computed as follows:

$$\%\ \text{scavenging ability} = \frac{\text{Absorbance of reference} - \text{Absorbance of sample}}{\text{Absorbance of reference}} \text{x} \frac{100}{1}$$

Monoamine Oxidase Inhibitory Assay

The extract's impact on MAO (EC 1.4.3.4) activity was assessed using a previously described methodology.[22]

The reaction mixture included, in short, 0.025 M phosphate buffer (pH 7.0), 0.0125 M semicarbazide, 10 mM benzylamine, 0.67 mg of the enzyme, and 0–100 µL of extract. Following a 30-minute incubation period, acetic acid was added, heated for three minutes in a boiling water bath, and then centrifuged. After 10 minutes of room temperature incubation, the resultant supernatant (1 mL) was combined with an equivalent volume of 2,4-dinitrophenylhydrazine and 1.25 mL of benzene. The benzene layer was separated and then combined with an equivalent volume of 0.1 N NaOH. After decanting, the alkaline layer was heated for ten minutes at 80 °C. A UV/visible spectrophotometer

(Jenway 6305 model) was used to measure the orange-yellow colour that formed at 450 nm. The percentage inhibition of the reference was then used to express the MAO activity.

In vitro antidiabetic assay

α-Amylase Inhibitory Potential

The experiment was carried out by the standard technique to ascertain the extracts' capacity to inhibit α-amylase.[22] First, 5 U/mL of the enzyme was prepared in ice-cold PBS at pH 6.7, containing 20 and 6.7 mM NaCl. Next, inhibitors (acarbose or test samples) were added to 250 µL of the enzyme at various doses (a blank sample was not included), and the mixture was incubated for 20 minutes at 37 °C. Next, a 0.5% (w/v) starch solution was added, and the mixture was heated to 10 minutes at 100 °C. Finally, the absorbance was measured at 540 nm.

α-Glucosidase Inhibitory Potential

The extracts' impact on intestinal α-glucosidase activity was assessed by measuring the amount of glucose produced by the breakdown of sucrose using a method outlined by Ogunlakin *et al*..[22] The test solution (10 I.U.) for the assay was made up of 100 µL of 50 mM sucrose, 1000 µL of phosphate buffer (50 mM; pH = 7.5), and 100 µL of α-glycosidase enzyme solution. Test samples, positive control (acarbose), or control (distilled water) were added to this mixture in different amounts. At 500 nm, the absorbance was measured.

In vivo assay

Dosing of experimental animals

The ethnobotanical survey conducted in Iwo, Nigeria, during the study (unpublished data) indicates that human medicinal dosages of Celosia argentea vary from 1 to 9 g. Rat dosage was calculated using the conversion factor from human to albino rat (conversion factor = 0.162) and body surface area. This was accomplished by dividing it by the weight of an adult human (60 kg) and then multiplying the result by a factor that took the animal's body surface area into account.[24, 25] As a result, the dosage of 100 mg/kg body weight was used over the entire investigation. Gavage was used to provide the dosage orally. The animal's most recent recorded body weight was used to compute individual dose volumes. Because people eat the plant as a vegetable, oral delivery was chosen.

Ethical approval and experimental animals

The Biochemistry program at Bowen University in Iwo provided 15 healthy female Wistar rats weighing between 190 and 200 g at 8 weeks of age. As stated in NIH Publication No. 80-23 amended, 1996, all experimental rats utilised in this work were treated in compliance with the guidelines set forth for animal management in research. The rats' experimental treatment (BUI/BCH/2025/001) complies with ARRIVE principles, according to the Institutional Animal Ethics Committee of the Department of Biochemistry at Bowen University, Iwo. In a hygienic, well-ventilated animal facility at Bowen University, Iwo, the Wistar rats were cared for and kept in plastic cages. Temperature and humidity levels, among other environmental factors, were suitably maintained. The rats had unlimited access to water and were fed regular pellet diet. All animals were acclimated for a week before to research, and a natural 12-hour light/dark cycle was observed.

MSG-Induced Uterine Leiomyoma Study

Female Wistar rats were grouped into 3 groups of 5 animals each. To assess the impact of Celosia argentea aqueous extract on uterine leiomyoma produced by monosodium glutamate (MSG), the study was divided into three groups. Group A (distilled water, 2 ml/kg) was the control group. To cause uterine leiomyoma, Group B received 800 mg/kg of MSG every day for 30 days. Group C received 800 mg/kg of MSG for 30 days in order to induce uterine leiomyoma, following the identical induction technique as Group B. Group C received daily treatment of 100 mg/kg of *C. argentea* extract for an additional 30 days after this induction period. At the conclusion of the experiment, the rats were put to sleep by intraperitoneal injection of sodium pentobarbital (40 mg/kg) 24 hours after the final treatment.

Hormonal analysis

Total Serum Follicle-stimulating Hormone (FSH)

Using a direct sandwich enzyme-linked immunosorbent assay (ELISA), follicle-stimulating hormone (FSH) levels were measured in accordance with the Calbiotech Inc. USA protocol (FS046F). Each sample was mixed with an anti-FSH-HRP conjugate and added to wells that had been previously coated with monoclonal anti-FSH antibodies for this assay. Any unattached proteins were eliminated by a washing process following incubation. Following the introduction of the substrate, a colorimetric reaction was started. Spectrophotometric measurements of the resultant colour intensity were made at a wavelength of 450 nm.

Luteinizing Hormone (LH)

A solid-phase enzyme-linked immunosorbent assay (ELISA), namely the Calbiotech Inc. kit (Calbiotech Inc, USA), was used to evaluate the serum levels of luteinizing hormone (LH). This assay uses a sandwich enzyme immunoassay approach in which the sample's LH binds to streptavidin-coated microwells. The substrate tetramethylbenzidine (TMB) is then added after a conjugate reagent. A spectrophotometer set to 450 nm is used to measure the colour intensity after an incubation period and subsequent washing to eliminate unbound components.

Estradiol Level

Serum estradiol (E2) concentrations were measured using a competitive binding enzyme-linked immunosorbent assay (ELISA) in compliance with the manufacturer's protocol provided by Calbiotech Inc. (Calbiotech Inc., USA). An anti-E2 antibody and an enzyme-linked estradiol conjugate were applied to each sample in this experiment. The conjugated antigen and the endogenous estradiol in the sample compete for the few accessible antibody binding sites. After the reaction was stopped using an acid solution, the absorbance at 450 nm was measured. It's interesting to note that the amount of estradiol in the sample was inversely correlated with colour intensity.

Testosterone level

Following the manufacturer's instructions, the DRG EIA-1559 ELISA kit (DRG Instruments GmbH, Germany) was used to measure testosterone levels. To put it briefly, each well set aside for standards, samples, and controls received 25 µL of blood plasma. Each well was then filled with 200 µL of the enzyme conjugate and gently stirred for 10 seconds. Following a 60-minute incubation period at room temperature, the plate was cleaned three times using 400 µL of wash buffer per well. The dish was thoroughly blotted with absorbent paper to guarantee total removal of any remaining liquid. Each well was then filled with 200 µL of substrate solution and left to react at room temperature for 15 minutes. Next, 100 µL of stop solution was added to each well to stop the enzymatic reaction. The xMarkTM Microplate Absorbance Spectrophotometer (Bio-Rad Laboratories Inc., USA) was used to detect absorbance at 450 nm. Microplate Manager® 6 software (Bio-Rad Laboratories Inc., USA) was used to calculate testosterone concentrations.

Harvest of Tissues for Biochemical Analyses

The euthanized animals' pancreatic and cerebral tissues (whole brain) were promptly removed, placed on ice, and weighed. This tissue was then homogenized in cold saline (1:10, w/v) using around ten up-and-down strokes at 1200 rpm in a Teflon-glass homogenizer. After centrifuging the homogenate for 10 minutes at 3000 × g to create a pellet that was discarded, a low-speed supernatant (S1) was kept.

Inhibition of Lipid Peroxidation

The lipid peroxidation test was conducted using a method outlined by Ogunlakin *et al*.[22] To put it briefly, 100 µL of S1 fraction was mixed with 30 µL of 0.1 M Tris–HCl buffer (pH 7.4), 30 µL of the extract (0–100 µL), and 30 µL of the pro-oxidant solution (7 mM sodium nitroprusside and 15 mM quinolinic acid). The volume was raised to 300 µL with water prior to an hour of incubation at 37°C. The colour reaction was produced by adding 500 µL of acetic acid/HCl (pH 3.4), 500 µL of 0.8% TBA (thiobarbituric acid), and 300 µL of 8.1% sodium dodecyl sulphate (SDS) to the reaction mixture containing S1. This mixture was incubated at 100ºC for one hour. The quantity of thiobarbituric acid reactive species (TBARS) was measured at 532 nm. Malondialdehyde (MDA) was then used to compare the absorbance to a reference curve.

Ovarian and Cervical Histology

After fasting for the entire night, the animals had a laparotomy to make it easier to remove their ovaries and cervixes. Using the usual histological procedure outlined by Avwioro26, the tissues' architecture was investigated using the Haematoxylin and Eosin staining technique. The collected tissues were meticulously cut into tiny pieces, each no thicker than 4 mm, and put into cassettes that had been marked beforehand. These pieces were then fixed in 10% formal saline for 24 h. 900 mL of purified water, 9 g of sodium chloride (NaCl), and 100 mL of 40% formaldehyde were combined to create the formal saline solution. The Leica TP 1020 tissue processor was used for automated tissue processing. Along with formal saline, a graded sequence of alcohol concentrations (70, 80, 90, and 95%) was used to dehydrate the materials. After being dehydrated, the tissues were put into metal molds, embedded in molten paraffin wax, and then placed on a cool plate to solidify. The paraffin blocks were taken out of the molds and cut to reveal the tissue surface once they had solidified. A rotary microtome was used to section the material at a thickness of 6 µm. After being further cut into 4 µm ribbon sections, these portions floated on a water bath that was kept at 55 °C (Raymond Lamb, address). After mounting the sections onto clean, labelled slides, they were dried for one hour at 60 °C on a hotplate (Raymond Lamb, UK) before being inspected using a light microscope with ×100 and ×400 objective lenses.

HPLC Analysis

To identify the phytochemical constituents present in the extracts, High-Performance Liquid Chromatography (HPLC) analysis was performed following the protocol described by Ogunlakin *et al*. [22] with slight modifications to optimize separation conditions. A reverse-phase C18 column (250 mm × 4.6 mm, 5 µm particle size) kept at a steady temperature of 30 °C was used for the analysis. Solvent A (water with 2% acetic acid) and solvent B (methanol) made up the mobile phase. They were applied in a gradient elution profile, beginning with 5% methanol for the first two minutes and increasing the concentration of methanol every ten minutes for the next ten to sixty minutes. Each sample had an injection volume of 20 µL, and the flow rate was set at 1.0 mL/min. A UV detector with a wavelength of 254 nm, which is appropriate for tracking a wide variety of phytochemicals, was used to detect the eluted molecules. Standard compounds for the presence of phenolic and flavonoid compounds in the extract included cinnamic acid, rutin, myricetin, gallic acid, caffeic acid, syringic acid, vanillin, p-coumaric acid, ferulic acid, ellagic acid, benzoic acid, catechol, p-hydroxybenzoic acid, vanillic acid, o-coumaric acid, salicylic acid, quercetin, naringenin, kaempferol, and apigenin.

Molecular Docking Studies

Protein structure preparation

The 3D structure of Dual Specificity Protein Phosphatase 6 (DUSP6) (PDB ID: 1HZM) [27] was retrieved from the Protein Data Bank (http://www.rcsb.org; accessed on 06/06/2025). The existing ligands and water molecules were removed from all the crystal structures, while missing hydrogen atoms were added using MGL-AutoDockTools (ADT, v1.5.6). [28]

Ligand preparation

The retrieval of the Structure Data Format (SDF) of HPLC-identified bioactive compounds from *C. argentea* was downloaded from the PubChem database (www.pubchem.ncbi.nlm.nih.gov; accessed in 06/06/2025). The compounds were further converted to the PDB chemical format using Open Babel.[29] Non-polar hydrogen molecules were merged with carbs, while the polar hydrogen charges of the Gasteiger-type were assigned to atoms. Furthermore, ligand molecules were converted to dockable PDBQT format with the help of AutoDock Tools.

Molecular docking of phytochemicals with the targeted active site

AutoDock Vina integrated with PyRx 0.8 was used to carry out an active site target molecular docking of the reference inhibitors and the HPLC-identified bioactive compounds to the binding site of the three target proteins.[30] Before the docking analysis, PyRx 0.8's bioactive chemicals were imported using OpenBabel..[29] OpenBabel was used to further reduce the bioactive chemicals. The Universal Force Field (UFF) and optimisation procedure were utilised as the energy minimisation parameter and conjugate gradient descent, respectively. Mapping the amino acid residues surrounding the native ligand's binding site allowed for the identification of the target proteins' binding site coordinates. Centre x (-0.50), y (0.02), z (0.051), and size x (42.35), y (40.67), z (36.36) were the dimensions of the grid boxes that were created. Using Discovery Studio Visualiser version 16, the chosen conformer from the docking analysis underwent additional interactive analysis.

Molecular Dynamics

For a 100 ns molecular dynamics simulation, the complexes of the two top-ranked docked bioactive compounds with DUSP6 were selected for further analysis. The study was conducted using GROMACS 2019.2 and the GROMOS96 43a1 force field.[31-33] The proteins' and ligands' topology files were generated using the Charmm GUI.[34,35] The simulation used a solvation system, periodic boundary conditions, physiological conditions, system minimization, and equilibration in a constant number of atoms, constant pressure, and constant temperature (NPT), all of which were similar to those in our previous study.[36-38] The temperature and pressure were kept at 310 K and 1 atm, respectively, using velocity rescales and a Parrinello-Rahman barostat. A leap-frog integrator was employed with a 2-femtosecond step. Snapshots were taken every 0.1 nanosecond for a total of 1000 frames per system throughout a 100 ns simulation. ROG, SASA, H-bonds, RMSD and RMSF, and MD trajectories.

Binding Free Energy Calculation using MM-GBSA

The Molecular Mechanics Generalized Born Surface Area (MM-GBSA) method and decomposition analysis using the gmx MMPBSA package were used to obtain the binding energies of amino acids within 0.5 nm of the ligand to determine the binding free energy of the two top docked phytochemicals from the initial docking analysis.[39-40] The methods used were the same as those published in our previous manuscripts.[36,37]

Statistical Analysis

One-way analysis of variance (ANOVA) was used to analyze the data, and GraphPad Prism version 5.01 for Windows (GraphPad Software, San Diego, California, USA) was used to compare group means using the Bonferroni test and Dunnett's Multiple Comparison Test. P-values less than 0.05 were considered significant. The values are displayed as Mean ± Standard Deviation (SD).

Results and Discussion

The antioxidant activity of the aqueous extract of *C. argentea* leaves is displayed in Table 1. When compared to quercetin, the standard utilized, the extract had a lesser capacity to scavenge DPPH radicals. Likewise, the NO radical ability was also lower than that of quercetin (Figure 1). Table 1 illustrates that the aqueous extract of *C. argentea* suppressed AChE activity with an IC_{50} of 0.098 ± 0.005 mg/mL, which is statistically significant when compared to the reference standard, donepezil (IC_{50} = 0.061 ± 0.009 mg/mL). Compared to quercetin, the extract had a reduced ability to chelate iron (Fe^{2+}). Figures 2(A) and 2(B) show how *C. argentea* leaf extract affects the activities of monoamine oxidase (MAO) and acetylcholinesterase (AChE). Both enzymes were inhibited by the extract in a concentration-dependent manner. Similar to donepezil (0.155 ± 0.005 µg/mL), *C. argentea* extract strongly reduced MAO activity in a concentration-dependent manner with an IC_{50} value of 0.178 ± 0.003 µg/mL (Table 2). Table 3 shows that the extract's α-amylase activity was slightly lower than the control's. Figure 3A shows an increase in α-amylase activity with increasing extract concentrations. The extract's ability to suppress α-glucosidase activity was less than the control in Figure 3B.

Fibrotic diseases, which affect organs including the uterus and cervix, are characterized by excessive extracellular matrix deposition and tissue scarring. According to Ashraf *et al*.,[41] there is growing evidence that oxidative stress plays a key role in fibrosis. The *C. argentea*'s ability to scavenge a variety of radicals, including DPPH, $NO^{\bullet}$, and $OH^{\bullet}$, indicates that it has broad-spectrum antioxidant potential. The most reactive ROS, OH radicals, directly denature DNA and proteins, hastening the remodeling of fibrotic tissue.[41,42] Since *C. argentea* could neutralize $OH^{\bullet}$, it may offer protection against fibroblast activation and collagen cross-linking caused by ROS. It is also essential to inhibit NO radicals because long-term overproduction of NO causes inflammatory cascades that are connected to pulmonary and pancreatic fibrosis.[43] The extract's pharmacological importance is shown by its notable performance

against common antioxidants, such as quercetin and ascorbic acid; yet variations in efficacy reflect the intricacy of interactions between natural compounds.[44] The anti-fibrotic potential of *C. argentea* is further enhanced by its MDA inhibitory impact in the rat brain and pancreas. One indicator of oxidative tissue damage is MDA, a byproduct of lipid peroxidation. The degree of fibrosis in neurodegenerative diseases and non-alcoholic fatty pancreatic disease (NAFLD) correlated with elevated MDA levels.[45] *C. argentea* may maintain membrane integrity and reduce lipid-peroxidation-induced apoptosis, halting the course of fibrosis, by inhibiting MDA production comparable to that of donepezil (a reference substance). This is relevant to pancreatic fibrosis, as oxidative stress speeds up ductal stiffness and acinar cell shrinkage.[46,47] Although this study provides empirical support for the antioxidant properties of *C. argentea*, computational methods may be able to reveal subtle molecular effects. The molecular docking models forecast how phytoconstituents such as flavonoids and saponins found in *Celosia spp*. will interact with fibrotic targets, such as TGF-β receptors or NADPH oxidase (NOX) enzymes. Multi-target effects, like concurrent ROS scavenging and NF-κB pathway inhibition, are further clarified by network pharmacology analyses.[48] One probable component, quercetin, for example, inhibits collagen formation by modulating Smad3 phosphorylation through computationally predicted binding.[43]

Table 1: IC_{50} values of the antioxidant potentials of *C. argentea* leaves aqueous extract

Samples	IC_{50} (mg/mL) DPPH scavenging	Fe Chelation	NO scavenging	OH radical scavenging	MDA (Brain)	MDA (Pancreas)
C. argentea	3.104±0.010*	0.281 ± 0.010**	0.836 ± 0.010**	5.279±0.010**	0.024 ± 0.002^{NS}	0.024 ± 0.005^{NS}
Standard(s)	0.311 ± 0.010^{Asc}	0.118 ± 0.010^{Q}	0.014 ± 0.010^{Q}	8.534 ± 0.010^{Q}	0.026 ± 0.002^{D}	0.026 ± 0.005^{D}

Asc =ascorbic acid; Q = quercetin; D = Donepezil; NS means there is no significant difference, and * and ** mean there is a significant difference compared to the standard. (n=3).

Table 2: IC_{50} values of acetylcholinesterase and monoamine oxidase inhibitory activity of *C. argentea* leaves aqueous extract

Samples	IC_{50} (mg/mL) Acetylcholinesterase inhibitory activity	Monoamine oxidase inhibitory activity
C. argentea	0.098 ± 0.005**	0.178 ± 0.003**
Standard	0.061 ± 0.009	0.155 ± 0.005

Standard = Donepezil; ** means there is a significant difference compared to the standard.(n=3).

Table 3: IC_{50} values of the antidiabetic activity of *C. argentea* leaves aqueous extract

Samples	IC_{50} (mg/mL) α-amylase inhibitory activity	α-glucosidase inhibitory activity
C. argentea	0.042± 0.004*	0.108 ± 0.005**
Standard	0.038±0.002	0.081 ± 0.005

Standard = Gallic acid; *, and ** means there is a significant difference compared to the standard. (n=3).

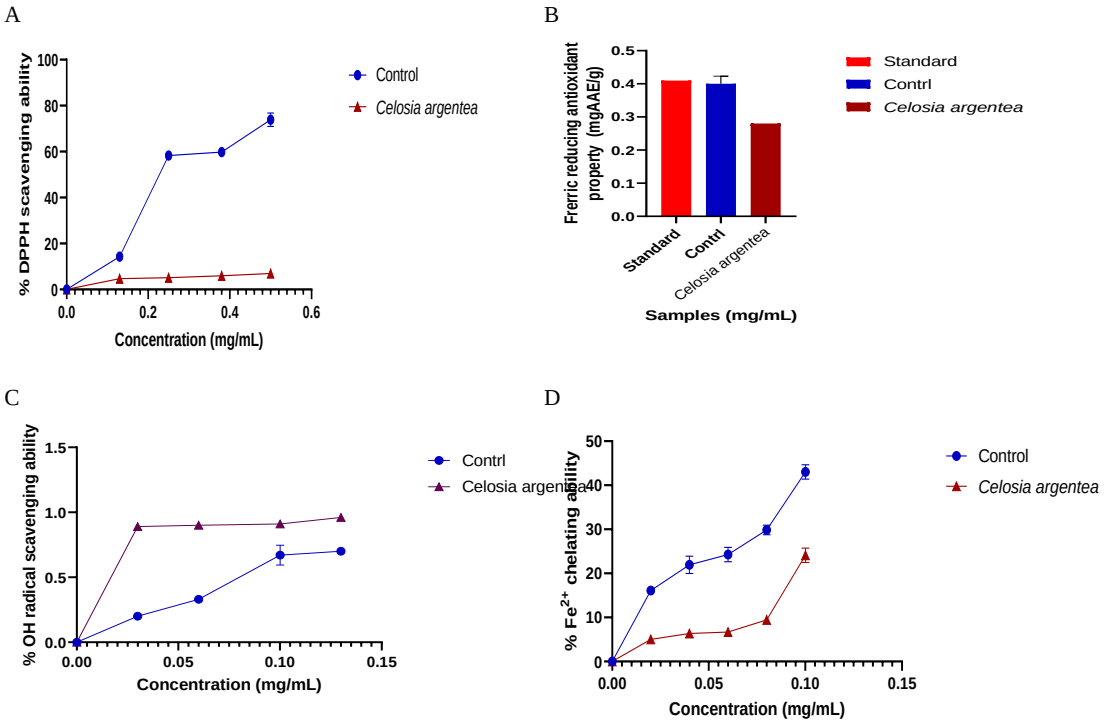

ISSN 2616-0684 (Print)
ISSN 2616-0692 (Electronic)

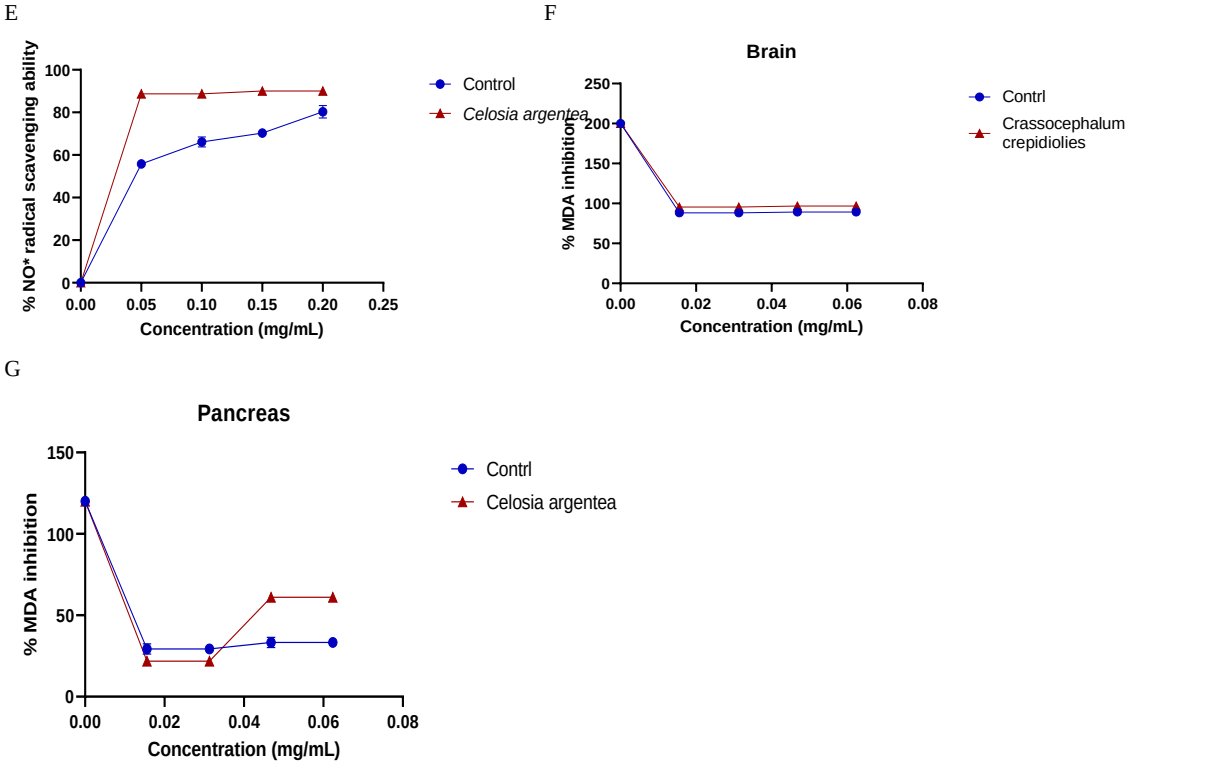

Figure 1: Percentage (A) DPPH radical, (B) Ferric Reducing antioxidant properties, (C) Hydroxyl radical scavenging ability, (D) Iron Chelating activity, (E) Nitric oxide radical scavenging ability, and Malondialdehyde Inhibitory effect (F) in brain and (G) pancreas tissue of C. argentea (n=3). Control for all is Quercetin, and DPPH radical assay, where ascorbic acid was used. Control for the MDA inhibition assay is Donepezil.

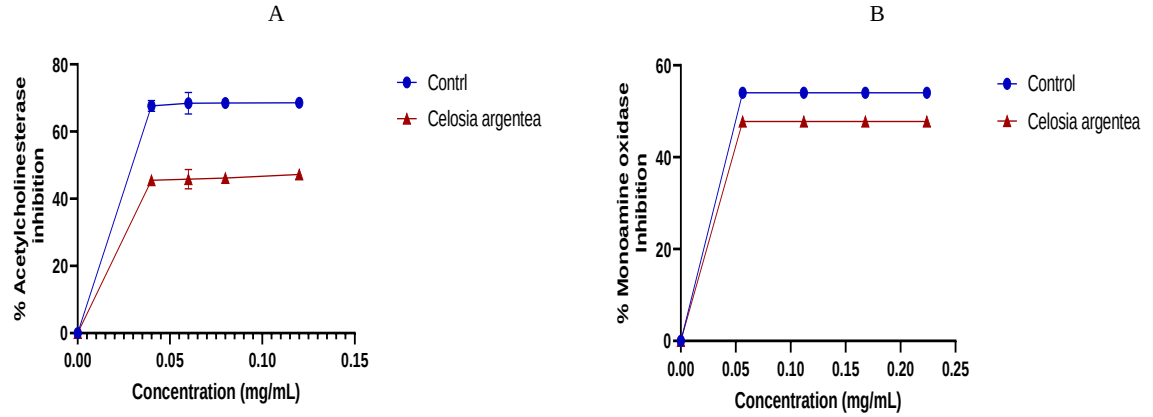

Figure 2: Percentage Acetylcholinesterase (ACHE) (A) and Monoamine oxidase Inhibitory (B) effects of *Celosia argentea* leaf. Control (Donepezil). (n=3).

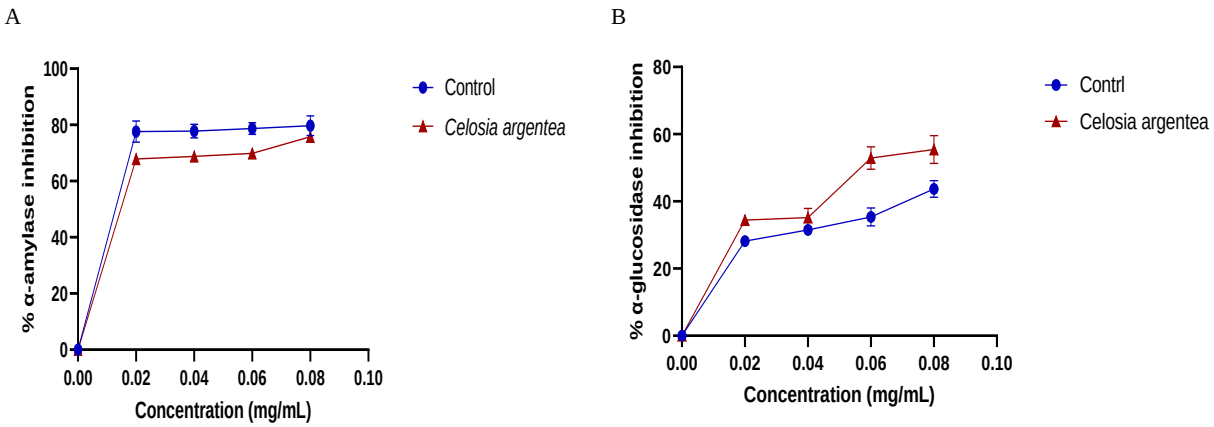

Figure 3: Percentage α-amylase (A) and α-glucosidase (B) Inhibitory effects of *Celosia argentea* leaf. Control (Gallic Acid). (n=3).

Celosia argentea has been documented in Indian folk medicine as a treatment for diabetes mellitus, reflecting its recognized antidiabetic properties.[49] Broader ethnopharmacological surveys indicate that over 1,200 plant species exhibit hypoglycemic activity, with ancient Indian literature citing more than 800 plants for antidiabetic applications.[50] Postprandial hyperglycemia is primarily mediated by two carbohydrate-

hydrolyzing enzymes: α-amylase, which initiates starch breakdown by cleaving α-1,4-glycosidic bonds to yield disaccharides, and α-glucosidase, which further hydrolyzes disaccharides to absorbable monosaccharides.[51] Inhibitors of these enzymes delay carbohydrate digestion, thereby attenuating postprandial glucose spikes. These enzymes are essential for the digestion of carbohydrates, and their inhibition can effectively lower postprandial blood glucose concentrations. This approach represents a fundamental strategy in the management of type 2 diabetes.[52] Research has assessed the *in vitro* inhibition of α-amylase and α-glucosidase by *C. argentea* leaf extracts, indicating its promise as an antidiabetic agent.[53] While ethanolic extracts of its roots, seeds, and leaves demonstrate antihyperglycemic effects in streptozotocin- and alloxan-induced diabetic rodents,[53] no prior studies have evaluated the enzyme-inhibitory activity of the aqueous leaf extracts. Moreover, the aqueous extraction is a better simulation of the natural way of human consumption of vegetables. Consequently, the present investigation specifically addresses this gap by analyzing α-amylase and α-glucosidase inhibition using aqueous extracts. According to our findings, the *C. argentea* leaf aqueous extract had 70% α-amylase inhibitory activity compared to the control at 79% and 50% α-glucosidase inhibitory activity compared to the control at 41%. As a control, gallic acid demonstrated α-amylase inhibitory activity at 79% and α-glucosidase inhibitory activity at 41%, respectively. In comparison to the control, which was 0.038 mg/mL for α-amylase and 0.081 mg/mL for α-glucosidase inhibitory activity, the IC_{50} value was 0.042 mg/mL for α-amylase and 0.108 mg/mL for α-glucosidase inhibitory activity. According to earlier studies, *C. argentea*'s complex phytochemical profile, especially its high flavonoid content, is largely responsible for its antidiabetic activity. Alkaloids, phenolics, triterpenoids, flavonoids, steroids, saponins, and tannins with antidiabetic properties have all been found in *C. argentea*[53] according to phytochemical investigations.[54].

Among the critical enzymes involved in the progression of neurodegenerative diseases are acetylcholinesterase (AChE) and monoamine oxidase (MAO). These enzymes regulate the synaptic concentrations of acetylcholine and monoamines, respectively, and their overactivity contributes to the symptomatic and pathogenic features of neurodegeneration.[57] Inhibiting AChE enhances cholinergic transmission, while MAO inhibition preserves monoamines like dopamine and serotonin, both of which are essential strategies in managing AD and PD. The present study demonstrates that aqueous leaf extracts of *C. argentea* possess substantial inhibitory effects on both AChE and MAO, providing evidence of its therapeutic potential in the management of neurodegenerative diseases. Though Donepezil exhibited stronger inhibition, the inhibitory potential of *C. argentea* extract is notable considering it is a crude aqueous extract.[22] This inhibition supports its traditional use in cognitive enhancement and aligns with studies highlighting the cholinesterase inhibitory effects of phytochemicals, particularly flavonoids and alkaloids.[58,59]

Similarly, the *C. argentea* extract exhibited MAO inhibitory activity mg/mL, compared to the standard Donepezil. This activity is particularly relevant in PD, where MAO-B inhibitors like selegiline are used to prolong dopamine activity and reduce oxidative deamination.[60] MAO-mediated oxidation of monoamines generates hydrogen peroxide, which contributes to oxidative stress and neurodegeneration.[61] The significance of dual AChE and MAO inhibition lies in the potential to modulate multiple pathological targets with a single agent. Several studies have explored plants like *Salvia officinalis* and *Melissa officinalis*, which similarly exhibit dual-enzyme inhibition, pointing to a holistic neuroprotective strategy.[62] The findings on *C. argentea* align with this paradigm. AChE inhibitory activity profile of *C. argentea* mirrors those reported for other medicinal plants. For instance, the methanolic extract of *Artemisia afra* exhibited an IC_{50} of 0.12 mg/mL for AChE inhibition.[63] Likewise, *Ocimum gratissimum* has been shown to inhibit MAO and AChE activities significantly, largely due to its rich eugenol and thymol content.[64]

Figure 4 showed that the MSG-induced uterine leiomyoma rats had a considerably greater level of testosterone, even though the luteinizing hormone (LH) levels in the MSG-treated group and the *C. argentea*-treated group differed significantly. The treatment group's lower levels of estradiol and testosterone compared to the control group showed that *C. argentea* significantly improved the hormonal abnormalities in the albino rats. The photomicrograph of the rats' uterus and ovaries is shown in Figure 5. In the ovarian cortex of the *C. argentea*-treated group, a photomicrograph of the ovary section revealed growing follicles, including primary, secondary, and antral follicles as well as a few Graafian follicles. The ovarian stroma displays luteinized cells and normal connective tissues (slim arrow). The *C. argentea*-treated group's cervix displayed a typical endometrial epithelial layer. Normal endometrial glands and a little inflammatory cell infiltration of the uterine stroma are present. The myometrium layer has a moderate level of vascular congestion.

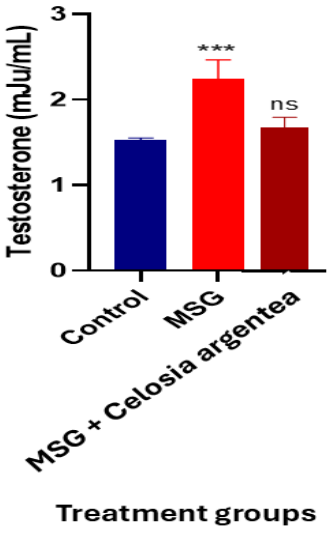

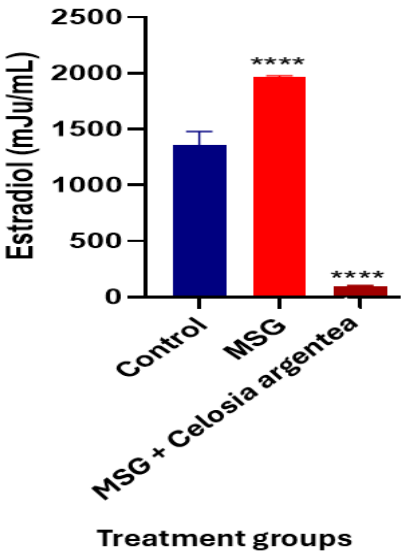

ISSN 2616-0684 (Print)
ISSN 2616-0692 (Electronic)

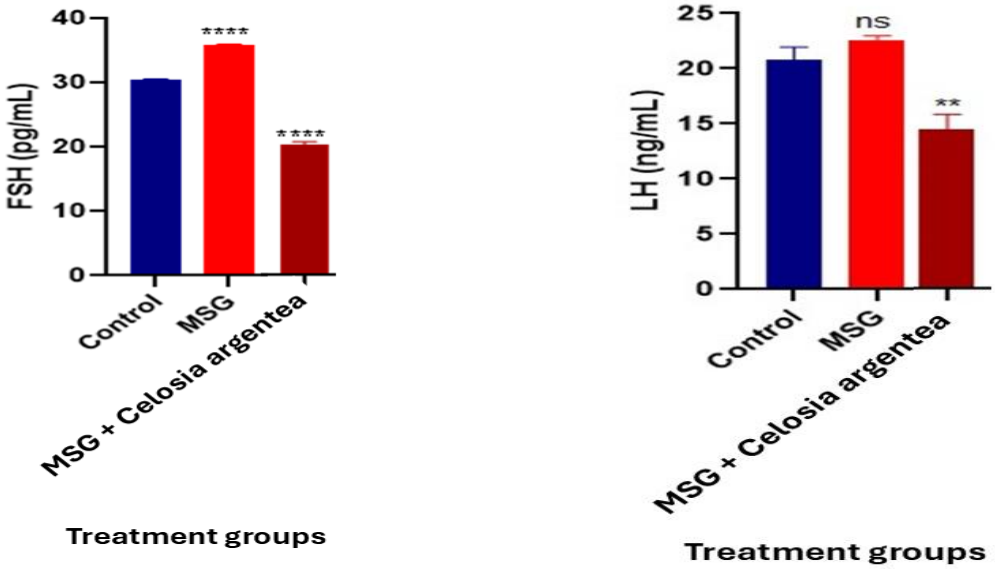

Figure 4: Effect of *C. argentea* leaf extract on FSH, LH, Testosterone, and Estradiol levels in control and treated rats. **, ***, and **** mean there is a significant difference compared to the positive control group. (n=5).

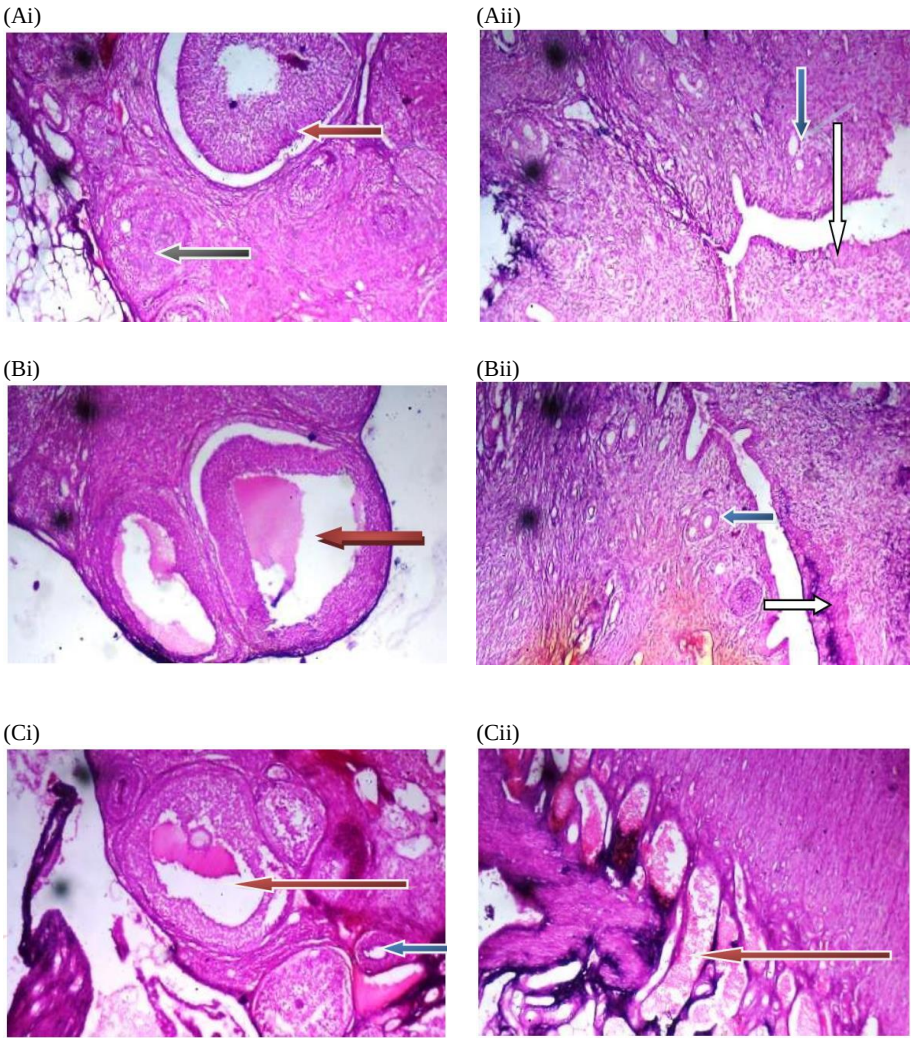

Figure 5: Photomicrograph of ovaries and uterine sections of the control (Ai and Aii), MSG-treated (Bi and Bii), and *C. argentea*-treated (Ci and Cii) groups, respectively, stained by hematoxylin and eosin (Mag. X 40). For the ovary, the Graafian follicle (red arrow), and Atresia follicle (black arrow) within the ovarian cortex, antral follicle with oocyte (green arrow). For the cervix, the endometrium epithelial layer (white arrow), normal endometrial gland (blue arrow).

The *in vivo* investigation provides compelling evidence for the therapeutic potential of *C. argentea* leaf extract in ameliorating MSG-induced uterine leiomyoma. The most striking finding of our study was the significant elevation of testosterone levels in MSG-treated animals, which aligns with previous research demonstrating MSG's disruptive effects on reproductive endocrinology.[65] This hormonal imbalance

represents a critical pathophysiological mechanism in uterine leiomyoma development, as elevated androgens can stimulate smooth muscle proliferation and alter the normal architecture of uterine tissue. The observation that MSG treatment led to hormonal dysregulation is consistent with an existing study that reported MSG administration significantly altered progesterone and estrogen levels in female rats, with concomitant changes in uterine morphology.[66] The remarkable ability of *C. argentea* extract to correct these hormonal anomalies is noteworthy. The treatment group showed substantially reduced levels of both testosterone and estradiol compared to the MSG-only group, suggesting that the plant extract possesses potent endocrine-modulating properties. This hormonal restoration is likely mediated through multiple pathways, given the complex phytochemical profile of *C. argentea*, which contains bioactive compounds including saponins, peptides, phenols, and amino acids.[67]

The mechanism by which *C. argentea* achieves this hormonal balance may involve its interaction with estrogen receptors and steroidogenic enzymes. Previous research has shown that MSG demonstrates high binding affinity to human estrogen receptors beta, potentially disrupting normal hormonal signaling pathways.[67] The saponins present in *C. argentea*, particularly the celosin compounds, may act as selective estrogen receptor modulators, helping to restore normal receptor function and downstream signaling cascades. This hypothesis is supported by the traditional use of *C. argentea* in Chinese medicine for treating reproductive disorders and its documented effects on hepatic pathogenic fire, which in traditional medicine theory is closely linked to hormonal regulation.[67] Furthermore, the normalization of luteinizing hormone (LH) levels suggests a partial restoration of hypothalamic-pituitary-gonadal axis function. This finding is particularly significant because LH plays a crucial role in ovarian steroidogenesis and follicular development. The incomplete restoration of LH levels may indicate that longer treatment duration or higher doses might be necessary to achieve complete hormonal normalization, or it could reflect the complex interplay between different hormonal pathways that require time to reestablish equilibrium.

The histopathological examination of ovarian and uterine tissues revealed remarkable improvements in the *C. argentea*-treated group, providing morphological evidence to support the biochemical findings. The presence of developing follicles at various stages, including primary, secondary, antral, and Graafian follicles within the ovarian cortex, indicates that the extract successfully preserved normal ovarian function despite MSG-induced stress. This finding is particularly significant because MSG has been shown to cause structural damage to reproductive tissues, including reduced lumen area and altered stromal architecture.[65] The observation of normal connective tissues and luteinized cells in the ovarian stroma of treated animals suggests that *C. argentea* extract possesses cytoprotective properties that extend beyond hormonal regulation. The luteinized cells are crucial for progesterone production and maintenance of reproductive cycles, and their preservation indicates that the extract may help maintain normal ovarian steroidogenic capacity. This morphological preservation correlates well with the hormonal improvements observed in our study and suggests that the therapeutic effects of *C. argentea* operate at both functional and structural levels. In the cervical tissue, the maintenance of normal endometrium epithelial layer and endometrial glands in the treated group represents another significant finding. The endometrium is highly sensitive to hormonal fluctuations, and its normal appearance in *C. argentea*-treated animals provides additional evidence for the extract's ability to maintain reproductive tissue integrity. The presence of only mild inflammatory cell infiltration in the endometrial stroma, compared to what would be expected in untreated MSG-exposed animals, suggests that the extract possesses anti-inflammatory properties that contribute to its overall therapeutic effect. The moderate vascular congestion observed in the myometrium layer of treated animals, while not completely normalized, represents a significant improvement over what would typically be seen in MSG-induced pathology. This finding suggests that *C. argentea* extract may help improve microcirculation in reproductive tissues, potentially through its antioxidant properties and ability to reduce oxidative stress-induced vascular damage.

The binding scores of the HPLC-identified compounds (Figure 6) against the DUSP6 target are represented in Table 4. Rutin stabilized in the binding to DUSP6 by a hydrogen bond with Thr149, Glu142, Ser144, Ala141, Leu27, Glu124, and pi-pi stacking. Chlorogenic acid interacted with DUSP6 via conventional hydrogen bonds with Ser144, Cys147, Glu148, Leu23, Trp22, Glu141, Ala141; pi-sigma interaction with Glue27 and pi-alkly contact with Ala21 (Figure 7). The molecular dynamics simulation showed a steady progression with observable convergence at the end of the simulation (Figure 8a). The plot of the RMSF system shows that high fluctuations were observed at the beginning of the simulation and around amino acid residues 27, 43, and 57 (Figure 8b). The DUSP6–Chlorogenic Acid complex with a mean RoG of 15.05 ± 0.12 Å was slightly lower than unbound, indicating increased structural tightness, while the DUSP6-Rutin system (15.13 ± 0.10) was also slightly lower than the unbound structure (Figure 8c). The graph showed that the ligand-bound complex and the free protein had somewhat different numbers of hydrogen bonds (Table 5). The mean and standard deviation (SD) of the various energy components that contribute to the binding free energy (kcal/mol) of the top docked molecules to 5kc5 are shown in Table 6. Figure 9 shows the molecular Mechanics Generalised Born Surface Area (MM-GBSA) plot of the amino acid residues that contribute to the DUSP6_Rutin and DUSP6_Chlorogenic acid complex.

Table 4: Binding scores of *C. argentea* identified bioactive compounds against DUSP6

SN	Compounds	Binding score (Kcal/mol)
1	Rutin	-7.5
2	Chlorogenic Acid	-7.2
3	Betalain	-6.7
4	Betandin	-6.6
5	Cristatain	-6.3
6	Rosmarinic Acid	-6.3
7	Catechin	-6.1
8	Quercitin	-6.1
9	Celogenamide A	-6
10	Epigallocatechin	-5.9
11	Gibberellic Acid	-5.9
12	Beta-Sitosterol	-5.7
13	Sitosterol	-5.7
14	Moroidin	-5.7
15	Caffeic Acid	-4.7
16	Amaranthin	-4.7
17	Dopamine	-4.5
18	Gallic Acid	-4.4
19	Butalimic Acid	-4.4
20	Celosin E	-4.1
21	4-Hydroxybenzoic Acid	-4

ISSN 2616-0684 (Print)
ISSN 2616-0692 (Electronic)

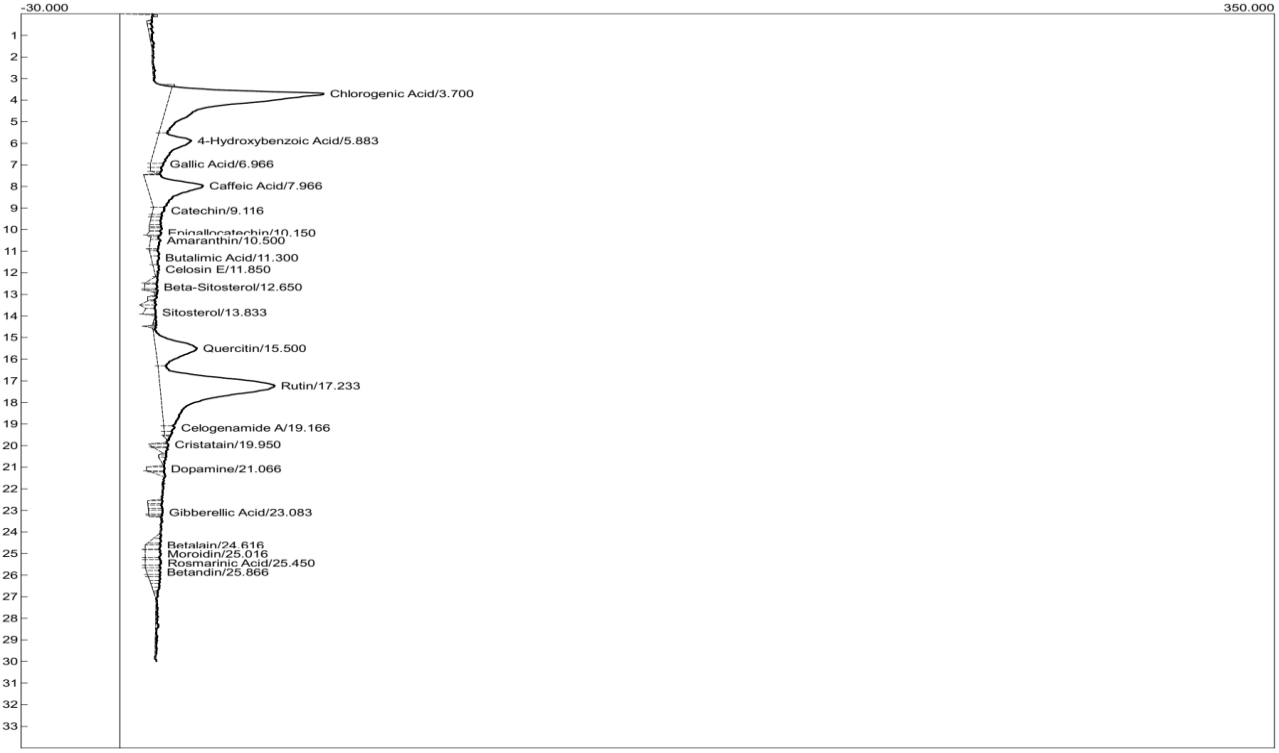

Figure 6: HPLC Chromatogram of *C. argentea* aqueous extract

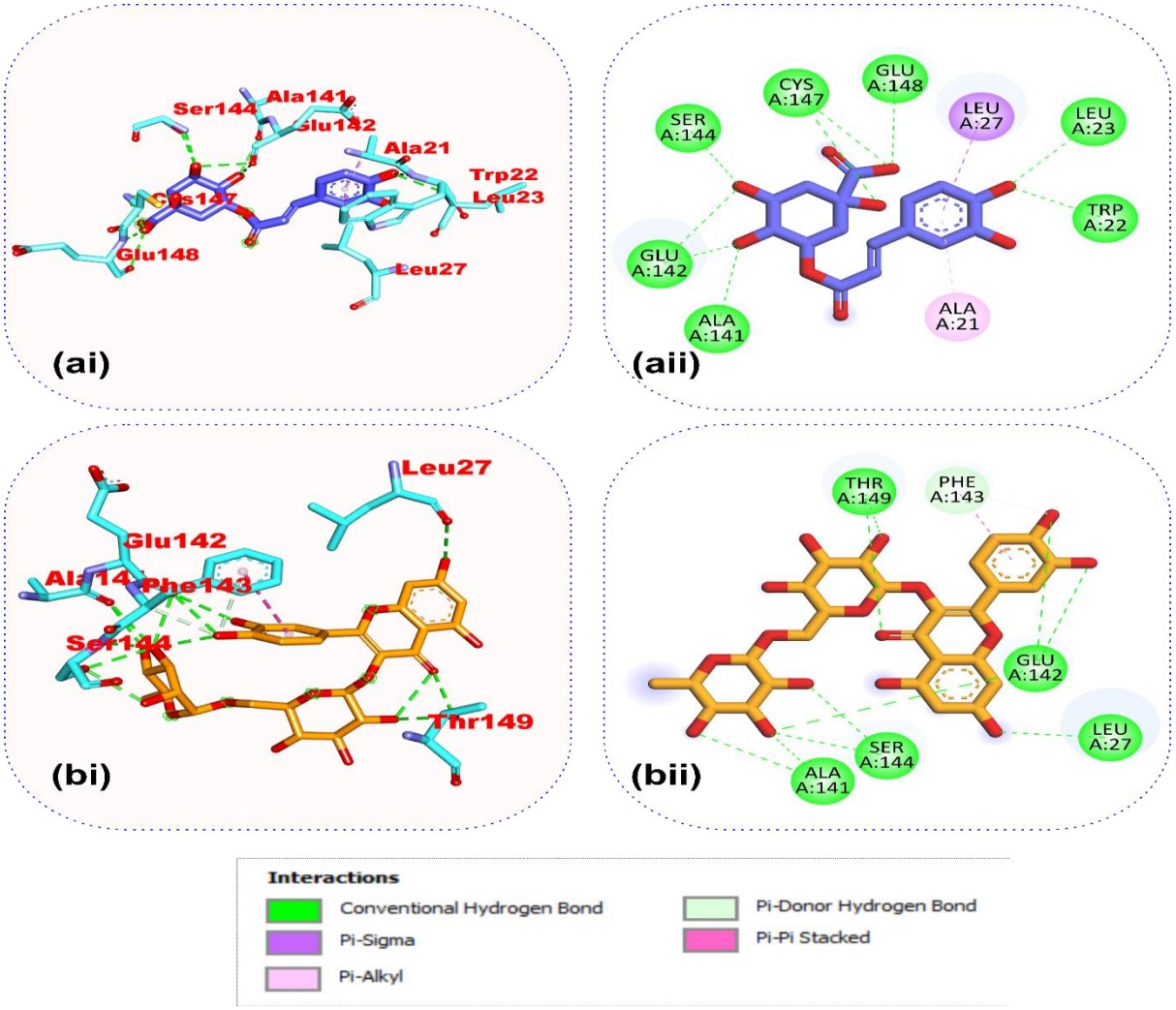

Figure 7: Interactive plots of top-ranked compounds from the docking analysis with amino acids in the binding site of Dual Specificity Protein Phosphatase 6 (DUSP6). The ligands are displayed as sticks. (a) Chlorogenic Acid (b) Rutin.

ISSN 2616-0684 (Print)
ISSN 2616-0692 (Electronic)

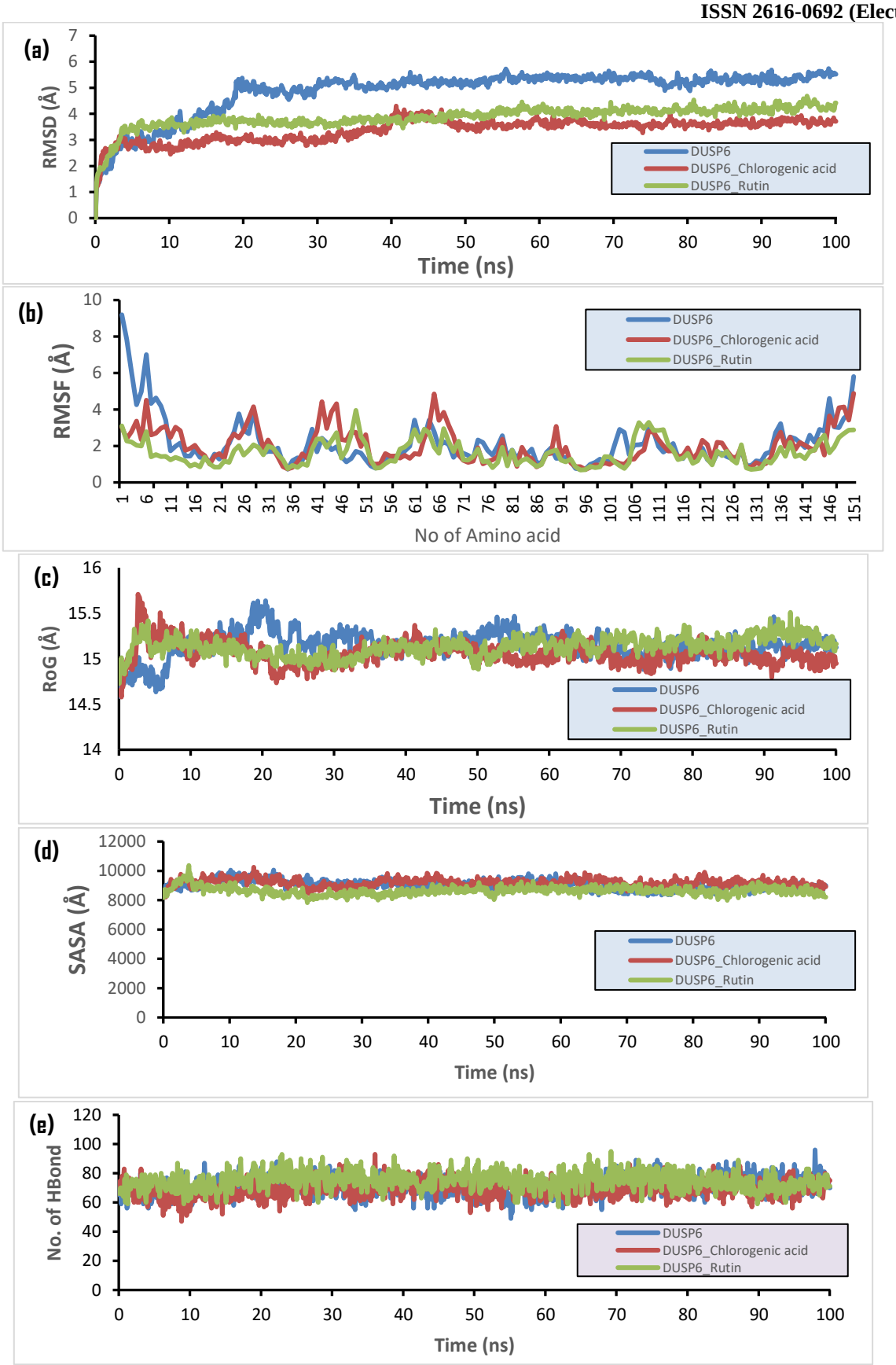

Figure 8: The plots of thermodynamic parameters computed from the analysis of the MDs trajectories of DUSP6 complex systems (a) The Backbone-Root Mean Square Deviation (RMSD) (b) Per residue Root Mean Square Fluctuations (RMSF) (c) radius of gyration (d) Surface Accessible Surface Area (SASA) (e) number of hydrogen atoms.

Table 5: The means and standard deviations of several parameters derived from the MDS trajectories of the highest-docked compounds complexed with their corresponding targets.

	Thermodynamic parameters				
Complexes	**RMSD (Å)**	**RMSF (Å)**	**RoG (Å)**	**SASA (Å^2)**	**H-Bonds**
DUSP6	4.87 ± 0.86	2.40 ± 1.63	15.15 ± 0.14	9028.74 ± 313.3	71.32 ± 6.44
DUSP6_Chlorogenic acid	3.37 ± 0.42	2.32 ± 0.98	15.05 ± 0.12	9187.66 ± 273.0	69.26 ± 5.95
DUSP6_Rutin	3.86 ± 0.42	1.72 ± 0.69	15.13 ± 0.10	8643.81 ± 279.1	74.62 ± 6.14

Table 6: The mean and SD of different energy components that make the binding free energy (kcal/mol) of top docked compounds to 5kc5.

SYSTEM	$\Delta_{VDWAALS}$	Δ_{EGB}	Δ_{EEL}	Δ_{ESURF}	Δ_{GGAS}	Δ_{GSOLV}	Δ_{TOTAL}
DUSP6_Chlorogenic acid	-19.48 ± 5.64	-77.86 ± 38.07	76.38 ± 29.51	-3.81± 0.80	58.37 ± 35.47	80.19 ± 29.60	-21.81 ± 9.135
DUSP6_Rutin	-34.24 ± 8.20	26.91 ± 11.92	-39.48 ± 9.85	-4.96 ± 0.99	-61.16 ± 14.53	34.51 ± 9.27	-26.65 ± 6.89

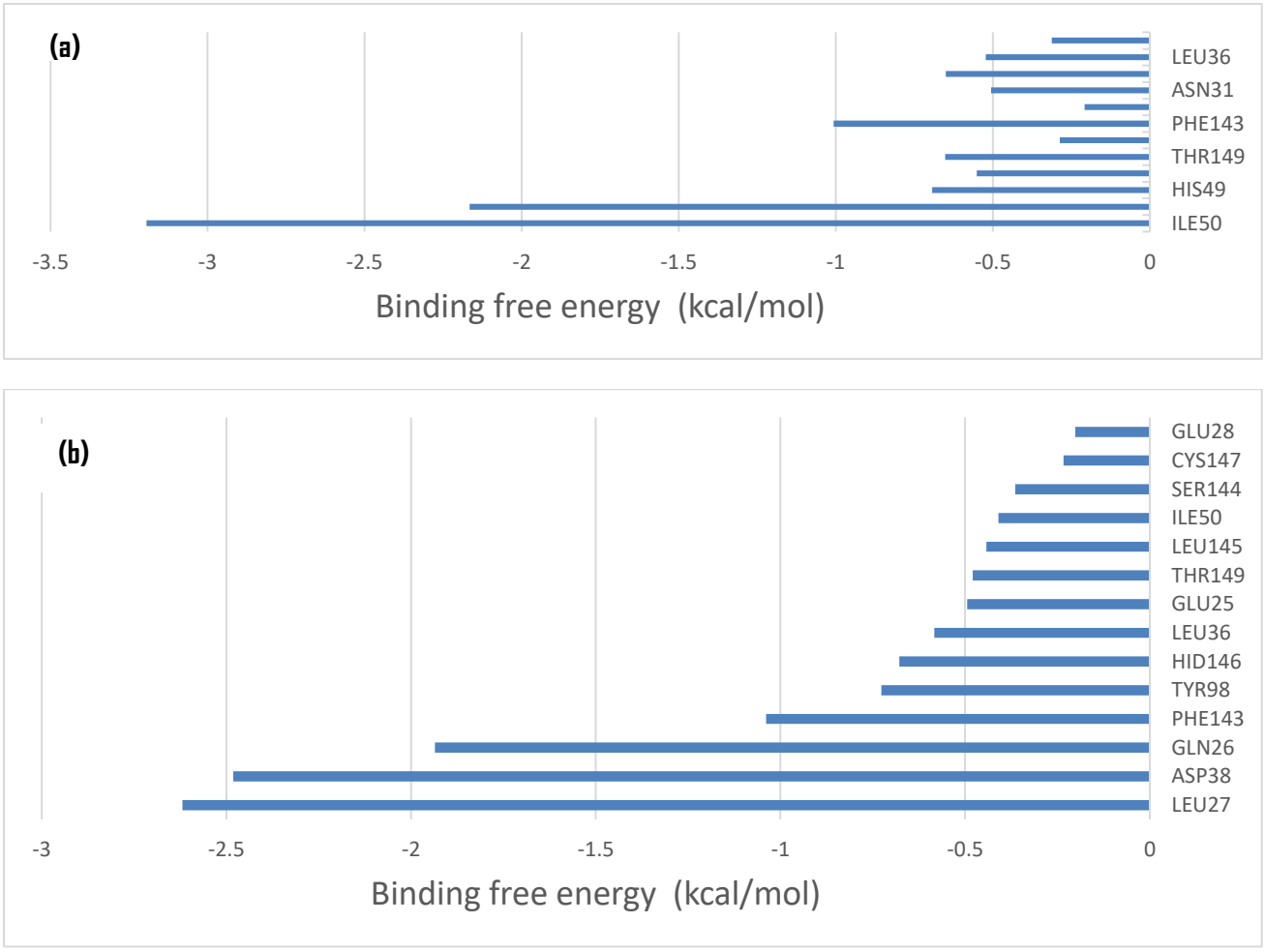

Figure 9: Molecular Mechanics Generalized Born Surface Area (MM-GBSA) plot of the contributing amino acid residues of (a) DUSP6_Rutin (b) DUSP6_Chlorogenic acid systems.

Dual Specificity Protein Phosphatase 6 (DUSP6) is a cytoplasmic phosphatase that selectively dephosphorylates and inactivates ERK1/2, key players in the MAPK pathway (Ahmad *et al.* 2018). Overactivation of ERK signaling is implicated in cancers and other proliferative diseases, such as fibroids (Bermudez *et al*., 2008). Therefore, inhibiting DUSP6 may sustain ERK activity. Docking ligands to DUSP6 helps identify potential modulators that can bind to its active site or regulatory pockets, thereby influencing its phosphatase activity. The binding scores were between -4 (4-Hydroxybenzoic Acid) and -7.5 (rutin) kcal/mol. The compounds with the most negative binding scores are rutin (-7.5 kcal/mol) and chlorogenic acid (-7.2 kcal/mol). These two compounds are likely to have the strongest predicted binding affinities with the target in comparison to the others. Betalain (-6.7 kcal/mol) and betanidin (-6.6 kcal/mol)—plant pigments with antioxidant properties; may stabilize binding via hydrogen bonds or π-π interactions. Cristatain, rosmarinic Acid, catechin, quercetin, celogenamide A presented binding scores around -6.3 to -6.0 kcal/mol, while caffeic acid, dopamine, gallic acid, butalimic acid, celosin E, and 4-hydroxybenzoic acid have binding scores between -4.7 and -4.0, likely to form weak, non-specific interactions. Generally, flavonoid and phenolic structures dominate the top hits, likely due to their multiple hydroxyl groups forming hydrogen bonds. Rutin and chlorogenic acid are promising and may serve as starting points for drug development or pharmacological validation. This structural diversity may lead to a variety of possible interactions with the target. Interactive analysis was applied to the two top-ranked compounds that were chosen based on the binding energy and interaction with the target. A hydrogen bond with Thr149, Glu142, Ser144, Ala141, Leu27, Glu124, and pi-pi stacking stabilized rutin's binding to DUSP6. Chlorogenic acid interacted to DUSP6 via conventional hydrogen bonds with Ser144, Cys147, Glu148, Leu23, Trp22, Glu141, and Ala141; pi-sigma interaction with Glue27 and pi-alkyl contact with Ala21. The strong interaction with the binding site residues of DUSP6 may stabilize the protein, thereby acting

as an activator, which is useful in ERK-overreactive proliferation, such as fibroids.

Molecular dynamics (MD) simulation is a crucial computational tool in studying ligand-protein interactions, providing insight into binding mechanisms, stability, and dynamic behavior at the atomic level.[68] The RMSD calculates the simulation's overall structural stability. A well-formed and stable complex is indicated by a decreased or steady RMSD.[68] The RSMD system was equilibrated for 20 ns. The baseline mean RMSD value for the 5KC5 (unbound) was 4.87 ± 0.86 Å. The DUSP6–chlorogenic Acid-bound (3.37 ± 0.42 Å) and DUSP6–Rutin (3.86 ± 0.42 Å). Complex presenting lower mean RMSD values when compared to the unbound system, indicate strong, stable interactions, potentially locking the protein into a conformation that could impact its enzymatic activity. The DUSP6–chlorogenic acid complex is the most stable, suggesting it is a promising modulator of DUSP6.[68] This stability supports its further evaluation in fibroid-related ERK signaling studies. The RMSF measures the flexibility of individual residues in the protein. Lower RMSF values suggest reduced flexibility and a more rigid structure.[69] The mean RMSF value of 2.40 ± 1.63 Å represents the baseline of the unbound system (DUSP6). The DUSP6–Chlorogenic acid system, with a mean RMSF value of 2.32 ± 0.98 Å, which is slightly lower, suggests that the ligand binding reduces local fluctuations of some of the regions of the protein. This implies that chlorogenic acid binds and stabilizes some regions, but not the entire protein. The DUSP6–rutin system (1.72 Å ± 0.69) presented the Lowest RMSF, suggesting strong and widespread stabilization of the protein structure. Indicates Rutin constrains flexible residues, possibly locking DUSP6 into a more rigid conformation.[70] RoG (Radius of Gyration) measures the compactness of a protein structure during molecular dynamics (MD) simulation. A higher RoG may suggest unfolding or structural expansion, while a lower RoG suggests a more stable, compact structure.[71] The mean RoG value of 15.15 ± 0.14 Å represents the baseline of the unbound system (DUSP6). The DUSP6-DUSP6-chlorogenic acid complex with a mean RoG of 15.05 ± 0.12 Å was slightly lower than unbound, indicating increased structural tightness, while the DUSP6-Rutin system (15.13 ± 0.10) was also slightly lower than the unbound structure. The binding of both ligands doesn't significantly alter global compactness but may stabilize local regions (as seen from the lowest RMSF). Together, chlorogenic Acid offers broad structural stabilization (lower RMSD and RoG), while rutin offers more localized, flexible residue stabilization (lowest RMSF).[72] Stabilization of DUSP6 can enhance its role as an ERK suppressor-critical in controlling fibroid cell proliferation.

The amount of protein surfaces exposed to the solvent is measured by SASA. More exposure is indicated by a higher SASA, whereas a more compact or buried building is indicated by a lower SASA.[73] The mean SASA value of 9028.74 ± 313.3 Å² represents the baseline of the unbound system (DUSP6). The DUSP6–chlorogenic acid system (9187.66 ± 273.0 Å²) caused a slight increase in the mean SASA value, indicating a slightly more exposed structure that may induce conformational opening. Since there is little change in SASA, ligand binding probably results in slight local structural changes rather than a significant shift in protein folding.[73] The binding of rutin to DUSP6 lowered the mean SASA value, indicating a more compact and less solvent-exposed complex. This may lead to better structural shielding from external denaturation forces, which can support protein activity and longevity.

Hydrogen bonds (H-bonds) are crucial for ligand-protein stability; a higher mean number indicates stronger interactions. The mean number of H-bonds, 72.2 ± 7.46, represents the baseline of the unbound system (DUSP6). The DUSP6_Chlorogenic acid (69.26 ± 5.95) shows a slight reduction in H-bonding relative to unbound DUSP6, suggesting minor disruption or rearrangement upon ligand binding. The DUSP6_Rutin (74.62 ± 6.14) forms the highest average number of hydrogen bonds, indicating potentially stronger or more stable interactions compared to the other systems.[73] Overall, both ligands—particularly Rutin, which exhibited a more favorable binding free energy—interacted strongly with the target, maintaining stable interactions throughout the simulation. The high-affinity binding of the top two ligands to DUSP6, coupled with the stabilized interaction, suggests that it may modulate the activity of the protein, which may interfere with cell proliferation and signaling, including fibroid cell survival, proliferation, or differentiation, and inflammation and fibrosis.[74]

The binding free energy quantifies the energy difference between the bound and unbound components of a complex (ligand and receptor); the greater the negative value, the higher the ligand's affinity for the protein.[75] Binding free energy estimates provide comprehensive information on the binding mechanisms of the top docked compounds throughout the early stages of drug discovery and development.[76] Using the MMGBSA method, the binding free energy of the two top docked compound against DUSP6 was evaluated. The DUSP6_rutin with a total binding free energy of -26.65 kcal/mol exhibits a more favorable (i.e., more negative) binding free energy than DUSP6_Chlorogenic acid (-21.81 kcal/mol), indicating stronger overall binding affinity. The gas-phase energy, which is a combination of Δ_{EEL} + $\Delta_{VDWAALS}$ of rutin (-61.16 kcal/mol), has a more favorable gas-phase interaction compared to chlorogenic acid (+58.37 kcal/mol). This indicates that electrostatic and van der Waals interactions drive the binding of Rutin, whereas chlorogenic acid has unfavorable electrostatics (high positive ΔEEL). Concerning solvation energy (ΔG_{SOLV}), which is a combination of Δ_{EGB} and ΔESURF, chlorogenic acid benefits significantly from solvation energy (-80.19 kcal/mol), counterbalancing its poor gas-phase interactions, while rutin, however, experiences desolvation penalties (+34.51 kcal/mol), possibly due to its bulk or polarity. Overall, while the binding of Chlorogenic acid is largely driven by solvation effects, the binding of rutin was dominated by strong van der Waals and electrostatic interactions in the gas phase. Overall, DUSP6_Rutin is predicted to bind more tightly than chlorogenic acid, with stronger gas-phase stabilization despite higher solvation cost.

The overall binding free energy was broken down into the individual contributing amino acids in order to determine how each amino acid contributed to the total binding free energy. Rutin was the most important residue for the DUSP6_rutin system in terms of electrostatic stabilization and van der Waals, suggesting a crucial involvement in binding. ASP38 is an electrostatically driven anchor, possibly forming a hydrogen bond or ionic interaction with the ligand. Residues like ILE50, LEU27, and LEU36 offer hydrophobic stabilization, supporting the binding pocket environment. Chlorogenic acid was the major contributor with (-9.639 kcal/mol). Strong positive electrostatic values (e.g., GLU25: +17.41, GLU28: +17.67) are counteracted by large negative polar solvation, resulting in a near-neutral or slightly negative net contribution. Hydrophobic residues (e.g., LEU27, LEU36, PHE143) primarily stabilized the ligand via van der Waals interactions. The decomposition reveals that ASP38, LEU27, and GLN26 are critical for ligand binding. These results are consistent with residues forming the binding pocket of DUSP6 and suggest a strong electrostatic and van der Waals synergy in stabilizing the ligand.

The hormonal fluctuations observed in this study underscore the need for more comprehensive mechanistic investigations to fully understand the pathways influenced by *Celosia argentea*. While our findings suggest promising therapeutic potential, future studies should explore concentration-dependent effects to determine optimal concentrations for efficacy and safety. Long-term evaluations in varied experimental models, including human clinical trials, are essential to establish translational relevance. Additionally, expanding molecular docking analyses to include a broader range of fibrotic targets will provide deeper insight into the compound's multi-target interactions. These computational predictions should be complemented by gene expression profiling and pathway analysis to validate biological relevance. Investigating the synergistic potential of Celosia argentea with other nutraceuticals or conventional therapies may further enhance its antifibrotic and hormonal regulatory effects. Such combinatorial approaches could lead to more effective, integrative treatment strategies for uterine leiomyoma and related disorders. Overall, while our study lays a foundational understanding of *Celosia argentea's* bioactivity, future research should aim to refine its therapeutic profile through rigorous pharmacological, molecular, and clinical assessments.

Conclusion

Celosia argentea improved fibrotic conditions in female Wistar rats, as evidenced by the antioxidant and antidiabetic properties presented herein. HPLC detected two important bioactive compounds: rutin and chlorogenic acid in the extract of *C. argentea*, and the plant's antifibrotic effect *in vivo* was corroborated by these compounds' significant binding affinity and stability with the protein target DUSP6. Collectively, the data imply that *C. argentea* may affect multiple targets in uterine fibroids, aiding the improvement of ovarian morphology, hormonal imbalance, and insulin insensitivity.

Conflict of Interest

The authors declare no conflict of interest.

Authors' Declaration

The authors hereby declare that the work presented in this article is original and that any liability for claims relating to the content of this article will be borne by them.

Acknowledgments

We appreciate Bowen University, Iwo, for supporting this study.

References

1. Pinto A. Uterine smooth muscle tumors: an overview. Adv Anat Pathol. 2024;31(6):397-410.
2. Giuliani E, As-Sanie S, Marsh EE. Epidemiology and management of uterine fibroids. Int J Gynecol Obstet. 2020;149(1):3-9.
3. Aninye IO, Chew S, Goulmamine S. 2025 SWHR Women's Health Research Agenda: prioritizing uterine fibroids, lupus, and metabolism. J Womens Health. 2025.
4. Sung JH, Kim KS, Han K, Park CY. Association of uterine leiomyoma with type 2 diabetes mellitus in young women: a population-based cohort study. Diabetes Metab J. 2024;48(6):1105-1113.
5. Anaziah G. The prevalence and post-operative complications of uterine leiomyomas in South-Western Nigeria and Northern Nigeria: a comparative review. 2023. [Accessed 2025 Apr 16].
6. Maekawa R, Sugino N. Epigenetics and uterine fibroids. In: Uterine Fibroids and Adenomyosis. 2018:69-85.
7. Glembocki AI, Somers GR. Prognostic and predictive biomarkers in paediatric solid tumours. Pathology. 2024;56(2):283-296.
8. Yang X, Chen Z, Qiu T, Liu Y, Ren H, Luo W, Zuo J, Li D. Lichong decoction improves inflammatory microenvironment and alleviates fibrosis in uterine leiomyoma via targeting CXCL8. J Ethnopharmacol. 2025;340:119276.
9. Sato S, Maekawa R, Yamagata Y, Tamura I, Lee L, Okada M, Jozaki K, Asada H, Tamura H, Sugino N. Identification of uterine leiomyoma-specific marker genes based on DNA methylation and their clinical application. Sci Rep. 2016;6:30652.
10. Kawanishi S, Ohnishi S, Ma N, Hiraku Y, Murata M. Crosstalk between DNA damage and inflammation in the multiple steps of carcinogenesis. Int J Mol Sci. 2017;18(8):1808.
11. Badulescu OV, Ciocoiu M, Vladeanu MC, Huzum B, Plesoianu CE, Iliescu-Halitchi D, Bojan A, Iliescu-Halitchi C, Bojan IB. The role of platelet dysfunctions in the pathogenesis of the hemostatic-coagulant system imbalances. Int J Mol Sci. 2025;26(6):2756.
12. Hu C, Chen Y, Yin X, Xu R, Yin C, Wang C, Zhao Y. Pancreatic endocrine and exocrine signaling and crosstalk in physiological and pathological status. Signal Transduct Target Ther. 2025;10(1):39.
13. Emerald M. Medicinal plants: therapeutic potential, safety, and toxicity. In: Drug Discovery and Evaluation: Safety and Pharmacokinetic Assays. Cham: Springer Int Publ; 2024:1327-1397.
14. Ajekiigbe VO, Agbo CE, Ogieuhi IJ, Anthony CS, Adewole OA, Ahmed B, Akingbola A, Nwankwo CK, Kayode AT, Chima UE, Adaobi OM. Innovative approaches to treatment of eye diseases: advances in stem cell therapy use in ophthalmology. Int Ophthalmol. 2025;45(1):113.
15. Krzyżanowski J, Paszkowski T, Woźniak S. The role of nutrition in pathogenesis of uterine fibroids. Nutrients. 2023;15(23):4984.
16. Lee J, Kim M, Son H, Kim S, Jo S, Janchiv A, Kim SY, Lee T, Yoo HY. Phytochemical characterization and bioactivity evaluation of extracts obtained via ultrasound-assisted extraction of medicinal plant Phedimus aizoon. Plants. 2024;13(14):1915.
17. Kawade S, Nagrik S, Sutar A, Daitkar S. Therapeutic potential of Celosia argentea in the management of urolithiasis: a comprehensive phytochemical and pharmacological review. Int J Sci Res Technol. 2025.
18. Tang Y, Xin HL, Guo ML. Review on research of the phytochemistry and pharmacological activities of Celosia argentea. Rev Bras Farmacogn. 2016;26:787-796.
19. Ibezute AC, Marcus-Abdul O. Exploring the lipid-modulating, haematological and antioxidant potential of Vernonia amygdalina and Celosia argentea in potassium bromate-induced toxicity in rats. Int J Res Innov Appl Sci. 2025;10(3):466-477.
20. Mueangnak K, Kitwetcharoen H, Thanonkeo S, Klanrit P, Apiraksakorn J, Klanrit P, Thanonkeo P. Enhancing betalains production and antioxidant activity in Celosia argentea vell suspension cultures using biotic and abiotic elicitors. Sci Rep. 2025;15(1):376. doi:10.1038/s41598-024-83096-x.
21. Fadogba OA, Ogunlakin AD, Ajayi AM, Sonibare MA. Antioxidant and anti-arthritic activity of Bombax buonopozense P. Beauv. leaves. Ann Pharm Fr. 2024;82(4):673-684.
22. Ogunlakin AD, Asaleye O, Anejukwo DS, Olusegun OV, Balogun H, Ayeni PO, Adeola AD, Gyebi GA, Adebodun GO, Molik ZA, Elbasyouni A. Understanding the mechanism of Crassocephalum crepidiodes (Benth.) S. Moore leaf antifibrotic activity using *in vivo* and in silico methods. Sci Rep. 2025.
23. Ogunlakin AD, Gyebi GA, Elbasyouni A, Awosola OE, Dada MM, Akinmurele OJ, Adegoke AA, Oladoja IK, Adelakun AD, Oluwadara O, Banwo GO. Ethnomedicinal validation of Telfairia occidentalis L. leaf: a dual experimental and computational approach to uterine leiomyoma therapy. Front Nutr. 2025;12:1669528.
24. Nair AB, Jacob S. A simple practice guide for dose conversion between animals and human. J Basic Clin Pharm. 2016;7(2):27.
25. Ogunlakin AD, Elagauma RO, Adegbenro AT, Olagookun FI, Adeyeye SA, Ojo OA, Awosola OE, Ogunlakin OA, Ezea BO, Paul-Adio VS, Sonibare MA. Assessment of nutritional, antioxidant, and antidiabetic properties of BF1 herbal formulation via in vitro and ex vivo approaches. Kuwait J Sci. 2025:100435.
26. Avwioro OG. Histochemistry and tissue pathology, principles and techniques. Claverianum, Nigeria; 2010.
27. Farooq A, Chaturvedi G, Mujtaba S, Plotnikova O, Zeng L, Dhalluin C, Ashton R, Zhou M-M. Solution structure of ERK2 binding domain of MAPK phosphatase MKP-3: structural insights into MKP-3 activation by ERK2. Mol Cell. 2001;7(2):387-399.
28. Morris GM, Huey R, Lindstrom W, Sanner MF, Belew RK, Goodsell DS, Olson AJ. AutoDock4 and AutoDockTools4: automated docking with selective receptor flexibility. J Comput Chem. 2009;30(16):2785-2791.
29. O'Boyle N, Banck M, James CA, Morley C, Vandermeersch T, Hutchison GR. Open Babel: an open chemical toolbox. J Cheminf. 2011;3(1):33.
30. Trott O, Olson AJ. AutoDock Vina: improving the speed and accuracy of docking with a new scoring function, efficient optimization, and multithreading. J Comput Chem. 2010;31(2):455-461.
31. Bekker H, Berendsen H, Dijkstra E, Achterop S, Vondrumen R, Vanderspoel D, Sijbers A, Keegstra H, Renardus M. GROMACS—a parallel computer for molecular-dynamics simulations. In: Proc 4th Int Conf Computational Physics (PC 92). World Scientific Publishing; 1993:252-256.
32. Oostenbrink C, Villa A, Mark AE, Van Gunsteren WF. A biomolecular force field based on the free enthalpy of hydration and solvation: the GROMOS force-field parameter sets 53A5 and 53A6. J Comput Chem. 2004;25(13):1656-1676.
33. Abraham MJ, Murtola T, Schulz R, Páll S, Smith JC, Hess B, Lindahl E. GROMACS: high performance molecular

simulations through multi-level parallelism from laptops to supercomputers. SoftwareX. 2015;1:19-25.
34. Lee J, Cheng X, Swails JM, Yeom MS, Eastman PK, Lemkul JA, Wei S, Buckner J, Jeong JC, Qi Y. CHARMM-GUI input generator for NAMD, GROMACS, AMBER, OpenMM, and CHARMM/OpenMM simulations using the CHARMM36 additive force field. J Chem Theory Comput. 2016;12(1):405-413.
35. Lee J, Hitzenberger M, Rieger M, Kern NR, Zacharias M, Im W. CHARMM-GUI supports the Amber force fields. J Chem Phys. 2020;153(3):035103.
36. Gyebi GA, Ogunyemi OM, Ibrahim IM, Afolabi SO, Adebayo JO. Dual targeting of cytokine storm and viral replication in COVID-19 by plant-derived steroidal pregnanes: an in silico perspective. Comput Biol Med. 2021;134:104406.
37. Ogunyemi OM, Gyebi GA, Ibrahim IM, Olaiya CO, Ocheje JO, Fabusiwa MM, Adebayo JO. Dietary stigmastane-type saponins as promising dual-target directed inhibitors of SARS-CoV-2 proteases: a structure-based screening. RSC Adv. 2021;11(53):33380-33398.
38. Ogunyemi OM, Gyebi GA, Ibrahim IM, Esan AM, Olaiya CO, Soliman MM, Batiha GE-S. Identification of promising multi-targeting inhibitors of obesity from Vernonia amygdalina through computational analysis. Mol Divers. 2023;27(1):1-25.
39. Miller BR III, McGee TD Jr, Swails JM, Homeyer N, Gohlke H, Roitberg AE. MMPBSA.py: an efficient program for end-state free energy calculations. J Chem Theory Comput. 2012;8(9):3314-3321.
40. Valdés-Tresanco MS, Valdés-Tresanco ME, Valiente PA, Moreno E. gmx_MMPBSA: a new tool to perform end-state free energy calculations with GROMACS. J Chem Theory Comput. 2021;17(10):6281-6291.
41. Ashraf H, Anushiravani A, Rayatpisheh M, Hamidi Alamdari D, Hossieni A, Kazeminezhad B. Association between oxidative stress and liver fibrosis severity in non-alcoholic fatty liver disease: insights from the pro-oxidant antioxidant balance method in a population from Tehran and Mashhad, Iran. Front Med. 2025;12:1539605. doi:10.3389/fmed.2025.1539605.
42. Rashid A, Khan MI, Choi JS. Red blood cell indices as biomarkers of oxidative stress: an overview. J Cell Biochem. 2020;121(5):4053-4062.
43. Zhao W, Bai B, Li H, *et al*. The role of oxidative stress-related genes in idiopathic pulmonary fibrosis. Sci Rep. 2025;15:5954. doi:10.1038/s41598-025-89770-y.
44. Divya BJ, Jyothi Sravani M, Hari Chandana J, Sumana T, Thyagaraju K. Phytochemical and phytotherapeutic activities of Celosia argentea: a review. World J Pharm Pharm Sci. 2019;8:488-505. doi:10.20959/wjpps20193-13312.
45. Babu PS, Kannan S, Reddy AP. Effects of Celosia argentea on haematological and biochemical parameters in experimentally induced oxidative stress. J Med Plants Res. 2021;15(10):276-285.
46. Gubergrits NB, Bieliaieva NV. Development and progression of pancreatic fibrosis: current concepts. Herald Pancreatic Club. 2025;67(2):22-37. doi:10.33149/vkp.2025.02.04.
47. Desai N, Sahel D, Kubal B, Postwala H, Shah Y, Chavda VP, Fernandes C, Khatri DK, Vora LK. Role of the extracellular matrix in cancer: insights into tumor progression and therapy. Adv Ther. 2025;8(2):2400370.
48. Franceschetti L, Bonomini F, Rodella LF, Rezzani R. Critical role of NF-κB in the pathogenesis of non-alcoholic fatty liver disease: a widespread key regulator. Curr Mol Med. 2021;21:495-505. doi:10.2174/1566524020666201026162343.
49. Vetrichelvan T, Jegadeesan M, Devi BAU. Anti-diabetic activity of alcoholic extract of Celosia argentea L. seeds in rats. Biol Pharm Bull. 2002;25(4):526-528.
50. Bhushan MS, Rao CHV, Ojha SK, Vijayakumar M, Verma A. An analytical review of plants for anti-diabetic activity with their phytoconstituents and mechanism of action. Int J Pharm Sci Res. 2010;1(1):29-46.
51. Matsui T, Tanaka T, Tamura S, Toshima A, Tamaya K, Miyata Y, Matsumoto K. α-Glucosidase inhibitory profile of catechins and theaflavins. J Agric Food Chem. 2007;55(1):99-105.
52. Yarizade A, Kumleh HH, Niazi ALI. In vitro antidiabetic effects of Ferula assa-foetida extracts through dipeptidyl peptidase IV and α-glucosidase inhibitory activity. Asian J Pharm Clin Res. 2017:357-360.
53. Telagari M, Hullatti K. In-vitro α-amylase and α-glucosidase inhibitory activity of Adiantum caudatum Linn. and Celosia argentea Linn. extracts and fractions. Indian J Pharmacol. 2015;47(4):425-429.
54. Sales PM, Souza PM, Simeoni LA, Magalhães PO, Silveira D. α-Amylase inhibitors: a review of raw material and isolated compounds from plant source. J Pharm Pharm Sci. 2012;15(1):141-183.
55. Tan MJ, Ye JM, Turner N, Hohnen-Behrens C, Ke CQ, Tang CP, Ye Y. Antidiabetic activities of triterpenoids isolated from bitter melon associated with activation of the AMPK pathway. Chem Biol. 2008;15(3):263-273.
56. Rohn S, Rawel HM, Kroll J. Inhibitory effects of plant phenols on the activity of selected enzymes. J Agric Food Chem. 2002;50(12):3566-3571.
57. Sharma K, Choudhary S, Kishore A. Neurodegenerative disease: pathophysiology, molecular mechanism and therapeutic approach. J Appl Biomed. 2020;18(3):105-111.
58. Orhan I, Kartal M, Naz Q, Ejaz A, Yilmaz G, Kan Y, Choudhary MI. Antioxidant and anticholinesterase evaluation of selected Turkish Salvia species. Food Chem. 2007;103(4):1247-1254.
59. López S, Bastida J, Viladomat F, Codina C. Acetylcholinesterase inhibitory activity of some Amaryllidaceae alkaloids and Narcissus extracts. Life Sci. 2013;71(3):2521-2529.
60. Youdim MB, Edmondson D, Tipton KF. The therapeutic potential of monoamine oxidase inhibitors. Nat Rev Neurosci. 2006;7(4):295-309.
61. Shih JC, Chen K, Ridd MJ. Monoamine oxidase: from genes to behavior. Annu Rev Neurosci. 1999;22:197-217.
62. Kennedy DO, Wake G, Savelev S, Tildesley NTJ, Perry EK, Scholey AB. Modulation of mood and cognitive performance following acute administration of single doses of Melissa officinalis (lemon balm) with human CNS nicotinic and muscarinic receptor-binding properties. Neuropsychopharmacology. 2011;28:1871-1881.
63. Oyedemi SO, Yakubu MT, Afolayan AJ. Anticholinesterase and antioxidant properties of Artemisia afra Jacq. Molecules. 2018;23(11):2899.
64. Ojo OA, Ojo AB, Ajiboye BO. Ocimum gratissimum leaf extract as a dual cholinesterase and monoamine oxidase inhibitor: in vitro evidence for its neuroprotective potential. Biomed Pharmacother. 2019;117:109088.
65. Abdulghani MA, Alshehade SA, Kamran S, Alshawsh MA. Effect of monosodium glutamate on serum sex hormones and uterine histology in female rats along with its molecular docking and in-silico toxicity. Heliyon. 2022;8(10):e.
66. Ajani OS, Obiechefu CH, Ake AS. Therapeutic effects of Cyperus esculentus on monosodium glutamate-induced haemo-biochemical and steroidogenic anomalies in male Wistar rats. Trop J Phytochem Pharm Sci. 2025;4(2):37-44.
67. Tang Y, Xin HL, Guo ML. Review on research of the phytochemistry and pharmacological activities of Celosia argentea. Rev Bras Farmacogn. 2016;26:787-796.
68. Elegheert J, Kakegawa W, Clay JE, Shanks NF, Behiels E, Matsuda K, Kohda K, Miura E, Rossmann M, Mitakidis N. Structural basis for integration of GluD receptors within synaptic organizer complexes. Science. 2016;353(6296):295-299.
69. Bornot A, Etchebest C, De Brevern AG. Predicting protein flexibility through the prediction of local structures. Proteins. 2011;79(3):839-852.
70. Narwani TJ, Etchebest C, Craveur P, Léonard S, Rebehmed J, Srinivasan N, Bornot A, Gelly JC, De Brevern AG. In silico prediction of protein flexibility with local structure approach. Biochimie. 2019;165:150-155.

71. Hong J, Gierasch LM. Macromolecular crowding remodels the energy landscape of a protein by favoring a more compact unfolded state. J Am Chem Soc. 2010;132(30):10445-10452.
72. Goldenberg DP. Computational simulation of the statistical properties of unfolded proteins. J Mol Biol. 2003;326(5):1615-1633.
73. Durham E, Dorr B, Woetzel N, Staritzbichler R, Meiler J. Solvent accessible surface area approximations for rapid and accurate protein structure prediction. J Mol Model. 2009;15:1093-1108.
74. Vastrad B, Vastrad C. Identification of novel prognostic targets in coronary artery disease and related complications using bioinformatics and next generation sequencing data analysis. bioRxiv. 2023 Feb 22:2023-02.
75. Du X, Li Y, Xia YL, Ai SM, Liang J, Sang P, Ji XL, Liu SQ. Insights into protein–ligand interactions: mechanisms, models, and methods. Int J Mol Sci. 2016;17(2):144.
76. Kollman PA, Massova I, Reyes C, Kuhn B, Huo S, Chong L, Lee M, Lee T, Duan Y, Wang W. Calculating structures and free energies of complex molecules: combining molecular mechanics and continuum models. Acc Chem Res. 2000;33(12):889-897.